processes

MDPI

Article

MULTITHMT: A MATLAB Application for Multidimensional Transient Heat and Mass Transfer Processes

M. Özgün Korukçu

Department of Mechanical Engineering, University of Bursa Uludag, Gorukle, Bursa 16059, Turkey; ozkorukcu@uludag.edu.tr; Tel.: +90-224-2941927

Abstract: Transient heat conduction and mass transfer have many applications in industry such as heating, cooling, cooking, quenching of steels, freezing, and convective drying of vegetables or fruits. A novel, interactive, and fast MATLAB application, named MULTITHMT, is improved to solve multidimensional transient heat and mass transfer problems. Exact solutions are obtained for infinite rectangular bars, short cylinders, rectangular prisms, and spherical geometries. Instantaneous temperature and moisture content at any location in the objects are obtained and temperature and moisture content at the final time are displayed in two- and three-dimensional graphics. Quenching of steel for rectangle bars and cooking of cylindrical or rectangular prism-shaped meat are represented for transient heat transfer. Cooling of spherical commercial bronze and iron is also investigated. For transient mass transfer, convective drying of rectangular prunes, bananas of short cylinders, and spherical cornelian cherries with different operational conditions is calculated. Drying of cubes with the same shape and different moisture diffusivities is investigated. MULTITHMT is the only program that uses exact solutions to calculate multidimensional heat and mass transfer problems in the available literature. It is also the only application that can calculate the target time with a given temperature or moisture content for any specific location in the studied multidimensional objects. This application can be used for educational purposes in several engineering departments and industrial applications where transient heat and mass transfer processes are needed.

Keywords: transient heat conduction; transient mass transfer; drying; application; multidimension; MATLAB

Citation: Korukçu, M.Ö. MULTITHMT: A MATLAB Application for Multidimensional Transient Heat and Mass Transfer Processes. *Processes* **2024**, *12*, 1411. https://doi.org/10.3390/pr12071411

Academic Editor: Ireneusz Zbicinski

Received: 12 June 2024
Revised: 1 July 2024
Accepted: 3 July 2024
Published: 6 July 2024



Copyright: © 2024 by the author. Licensee MDPI, Basel, Switzerland. This article is an open access article distributed under the terms and conditions of the Creative Commons Attribution (CC BY) license (https://creativecommons.org/licenses/by/4.0/).

1. Introduction

In modern engineering education, it has become inevitable to use computer-aided programs in addition to classical methods. It enables students, especially at the undergraduate level, to learn both the fundamentals of classical education and to reinforce this knowledge with modern educational tools, enabling them to learn knowledge permanently. The heat transfer course, which has many applications in engineering, is a basic course taught in many engineering departments. The subject of heat conduction in the transient regime, which is included in heat transfer courses, is used in many applications such as the thermal processing of metals, freezing, and preservation of fresh vegetables and fruits, and baking of food. Mass transfer is usually accompanied by heat transfer. Mass transfer can be due to the motion of a bulk fluid or due to mass diffusion. The general processes of mass transfer are drying, evaporation, absorption, distillation, precipitation, and membrane filtration. Mass transfer course is also taught in several engineering disciplines such as chemical and mechanical engineering. There are generally three approaches to solving heat and mass transfer problems. These are analytical, experimental, and numerical methods. Analytical methods are valid for simple problems, while experi-

ments give more realistic results, but the experimental setup is expensive and time-consuming. For these reasons, numerical methods are used as an alternative to analytical and experimental methods.

The easiest way to solve the transient heat conduction problem is to use the Lumped System Approach where there is a negligible temperature gradient in the system. When $Bi \leq 0.1$ Lumped System Approach can be used. This approach is easy and fast to calculate but when $Bi > 0.1$ the Heisler diagrams can be used to solve heat conduction problems in the transient regime [1,2]. Heisler presented diagrams for slabs, infinite cylinders, and spheres to determine the entire temperature profile in these geometries during heating or cooling processes. In the same study, another chart for finding heating times for short cylinders was also presented [3]. To find the temperature or time for heating and cooling processes by using Heisler charts is easy but not accurate. Reading errors may occur and another problem is with the Fourier number in the vicinity of 0, where the lines are not reaching 0 or too dense. To eliminate reading errors exact solutions can be used. Temperature values from the center to the surface of infinite slabs, long cylinders, and spheres were represented in charts [4]. The exact solutions for transient heat conduction problems can be found in Schneider [5]. An alternative method to solve transient heat conduction problems is to use the famous "one-term approximation". If the dimensionless Fourier number is greater than 0.2, this approximation can be used. This method takes only the first term of the exact solutions and truncates the higher-order terms. By using this approximation, the maximum error is lower than 2% [1].

Many researchers have worked on the numerical solution of heat conduction in a transient regime. One of the oldest studies among them was the study of Baughn and Rossi [6]. In their study, they used spreadsheets to solve one and two-dimensional transient heat conduction problems in Cartesian coordinates. Simple single-term approximations to solve the transient heat conduction problems were proposed by Yovanovich [7]. Explicit and accurate solutions to find the first roots of the Biot number for infinite plates, infinite circular cylinders, and spheres were presented. Accurate polynomial expressions for zeroth and the first kind of Bessel functions were developed. Developed expressions are expanded in trigonometric functions and these functions are presented in MapleV R3 spreadsheets. According to the calculations of the study, the maximum error is 1% of the exact series solutions. McMaster et al. [8] computed the temperature and heat transfer rate of parallelopiped under transient conditions by using FORTRAN. COND3D had boundary conditions such as constant surface temperature, constant heat flux, and heat convection. Two forms of Green functions, short- and long-term, were used. Another spreadsheet modeling to solve the three-dimensional transient heat conduction problem in Cartesian coordinates was proposed by Antar and Mokheimer [9]. In the study, the transient heat conduction equation was solved implicitly by using user-defined macros. Constant heat flux, constant surface temperature, thermal insulation, and thermal radiation boundary conditions could be applied to the problem. Zheng and Keith [10] developed a JAVA applet to solve the one-dimensional transient conduction-diffusion problem. The applet was based on reading Heisler charts in a graphical user interface (GUI). The user entered the input parameters and then read the necessary parameters from the screen. Their applet can be used for slab walls, infinite cylinders, and spheres. Ayatollahi et al. [11] developed a MATLAB-based GUI to calculate transient heat conduction for regular-shaped three-dimensional objects. In the study, the three-dimensional heat conduction equation was discretized by the forward finite difference method, and an explicit scheme was used to calculate the problem for time. With the help of the software, the users could calculate temperature values for a given time for the cylindrical and Cartesian geometries. They also verified their results with the results for the same problem with Fluent v5.2 software and found that the results were in good agreement. Li et al. [12] presented a meshless local Petrov–Galerkin (MLPG) method to solve the two-dimensional transient heat conduction in Cartesian coordinates. Local weak forms were developed using the weighted residual method locally from the partial differential equation of transient heat conduction. For

time-step calculations Modified Precise Time Step Integration Method (MPTSIM) was used. The proposed solution method was tested for a two-dimensional closure and compared with the analytical solution. The results were very close to the analytical solution. Yang et al. [13] proposed a novel numerical method, the Element Differential Method (EDM), to solve transient heat conduction problems with variable thermal conductivity. The method was based on the direct differentiation of shape functions of isoparametric elements used to evaluate the geometry and physical variables. Spatial discretization was carried out by using the central differencing scheme (CDS). Time marching was calculated by an implicit backward differentiation scheme. This scheme was unconditionally stable. The proposed method was compared with a 2D square and a 3D radiator with convection. The results were reliable with analytical and Finite Element Method solutions. Another study using EDM to solve multi-dimensional transient nonlinear heat conduction problems with heat sources was conducted by Cui et al. [14]. According to the study, to code EDM is easy with discretizing the differential equations by using the central differencing scheme and iterations to deal with nonlinearity. They presented solutions for 2D and 3D examples of their approach and verified with ANSYS Finite Element Method results. The only disadvantage of this approach was the developed code required very long computation times than FEM simulations when heat sources were used. Adsul and Dineshkumar [15] developed a fully explicit transient heat conduction solution for 2D composite walls by using C++. They compared the results of their code with a uniform 10 × 10 grid solution of the commercial software Fluent and showed that the developed code was calculating almost the same results as that of Fluent. Chiba [16] presented an analytical solution to solve transient heat conduction in composite slabs with time-dependent heat transfer coefficient boundary conditions. The solution was constructed in two steps. In the first step, the shifting function was used to derive new differential equations, and in the second step, the derived differential equations were solved by the orthogonal expansion technique. The method could also be applied to simple geometries with slight modifications.

There was also some software developed to solve transient heat conduction problems. Velazquez et al. [17] proposed educational software to simulate the transient heat transfer process in simple fin geometries. One dimensional heat conduction equation was modeled by using an equivalent network model. Prodasim 1 was solved by a network simulator which had different boundary conditions for the base, lateral surface of the fin, and the tip of the fin. By using the software, the authors also presented a case study to find the optimal length for a circular fin. Interactive software for solving transient heat conduction in cylindrical bodies was developed by Janáčová et al. [18]. The exact solutions for the infinite cylindrical system were obtained by Maple software. The natural convection heat transfer coefficient values were calculated by Nusselt correlations taken from the available literature. 2D and 3D visualization of temperature values in the cylinder could be obtained by the software. The authors reported that they have used the software in Process Engineering lectures for educational purposes. Another educational software for transient heat conduction problems was presented by Herazo et al. [19]. The exact solutions for infinite cylinders, semi-infinite solids, and spheres were obtained by using MATLAB software. These three cases were tested to evaluate the goodness of the software on selected students in Universidad del Atlantico. After the pretest and post-test results, the students gave positive feedback that they obtained better critical thinking, meaningful learning, and understanding of the fundamentals of transient heat conduction in heat transfer courses. Cantillo et al. [20] developed software for lumped system analysis and one-dimensional plane walls with Python. The transient heat conduction equation was solved by using the explicit finite difference method. The GUI, named DynamicHT was tested among three students and the statistical results showed that the proposed software had a significant effect on students understanding the transient heat conduction problems. Obregon et al. [21] presented a parametric study of transient heat conduction for infinite slabs, long cylinders, and spheres. A MATLAB-based GUI was used to solve exact solutions of equations. The heat transfer rate and temperature variation with time were presented for

pure aluminum, pure iron, and stainless steel. In the study, the effect of different heat transfer coefficients on heat transfer rate and temperature with time was also investigated.

Storing food by drying is an old technique that people have been using for ages. Drying is an intensive energy energy-consuming process therefore calculating the appropriate drying time in the drying industry plays an important role. Drying processes and the effects of drying techniques on dried product quality were studied by Strumillo and Adamiec [22]. Akter et al. [23] reviewed research on mathematical modeling for the drying of fruits and vegetables with a special emphasis on the computational approach. Different mathematical modeling approaches to solve heat and mass transfer phenomena as well as computational fluid dynamic methods were briefly described. The authors also reported that numerical models and computational modeling could be alternatives to time-demanding experimental studies. Kaya et al. [24] conducted experiments and numerical simulations for the drying of Hayward kiwi fruits. In the experiments, different drying conditions such as air velocity, temperature, and relative humidity were investigated. For numerical simulations, they used Fluent commercial software. After determining local distributions of the heat transfer coefficient, they obtained mass transfer coefficient values by using the Chillton–Colburn analogy. Moisture distributions in drying kiwi fruits were presented for different drying conditions. Computational modeling of the transport phenomena occurring during convective drying of prunes investigated by [25]. The author used COMSOL Multiphysics commercial software to solve transient partial differential equations. The shrinkage effect was also included in computational calculations. Experiments were conducted to validate the simulations. The parametric study revealed critical operation parameters for the drying of prunes. The parallel flow mode of drying resulted in a 20% shorter drying time than the counter flow mode of drying to reach the target moisture content in the prunes. Lemus-Mondaca et al. [26] presented a coupled 3D heat and mass transfer model for drying Chilean papaya fruit slices. The transport equation in 3D with time was solved by using the Finite Volume Method (FVM) with FORTRAN language. Computational results were validated with 2D and 3D experimental results. Various drying temperature values were applied and the effects on drying time were presented. Sabarez [27] investigated the mathematical modeling of coupled transport phenomena and color development of Trellis-Dried sultanas. For computations, the FDM method was used and an implicit solution scheme was used. Experimental results were compared with numerical solutions and it has been found sufficiently accurate. Kumar et al. [28] studied a multiphase porous media model for intermittent microwave convective drying (IMCD) of food. The multiphase medium consisted of liquid water, gases, and the solid matrix inside the food. For numerical calculations, COMSOL 4.4 software was used. The numerical calculations were compared with experimental moisture and temperature data that showed good agreement. Drying kinetics and modeling of mass transfer in thin layer convective drying of pineapples were investigated by Reddy et al. [29]. Air velocity was kept at 1.5 m/s and drying temperature values were taken as 55–60–65–70 and 75 °C, respectively. Drying calculations were conducted by using COMSOL software. Simulation results were compared with the available experimental data and the results showed that moisture ratio with drying time fitted with experimental data. Seyedabadi et al. [30] investigated convective drying simulation of banana slabs considering non-isotropic shrinkage using FEM with the Arbitrary Lagrangian–Eulerian method. The shrinkage of the bananas was experimentally calculated by using image processing techniques by taking photos of banana slices every 30 s. Heat and mass transfer equations were solved by using COMSOL Multiphysics 5.1 software. A strong linear relationship with experimental and numerical results for 70–80 and 90 °C drying temperature values. Rahman et al. [31] proposed a micro-level transport model for plant-based food materials during drying processes. Yuan et al. [32] investigated numerical and experimental studies on drying shrinkage-deformation of apple slices during the process of heat-mass transfer. The researchers conducted heat-mass transfer calculations coupled with a stress–strain mathematical

model and solved them by using COMSOL Multiphysics software. According to their results, the temperature distribution and moisture distribution of apple slices during the hot-air drying process were uniform. The peak values for thermal stress and moisture stress were occurred at the middle period of the whole drying process. The moisture stress caused by moisture gradient was higher than the thermal stress caused by temperature gradient. Boureima et al. [33] modeled the convective drying of tomato slices with COMSOL software. The experiments were conducted in a tunnel dryer with using values of 0.1 m/s, 0.25 m/s and 0.5 m/s for the drying air velocity and 50 °C; 60 °C for air temperatures. Their experimental results showed that the Root Mean Square Error (RMSE) was 8% with comparison to theoretical results. Rani and Tripathy [34] modeled the moisture migration during convective drying of pineapple slice considering non-isotropic shrinkage and variable transport properties. The shrinkage effect was accommo- dated into FE modelling using the arbitrary lagrange-eulerian method. COMSOL software was used for FE modeling of heat and mass transfer calculations. The results revealed that variable diffusion coefficient showed better results than constant diffusion coefficient. On the other hand, constant or variable mass transfer coefficient predicted similar results. Turkan and Etemoglu [35] numerically investigated wood drying. In their study, first flow and temperature field was obtained by using ANSYS-Fluent software, then heat and mass transport phenomena calculated by using COMSOL Multiphysics Software. Different air velocity and drying temperature values were used. Transient temperature and moisture distributions inside the solid were obtained. The comparison of their simulation results were reliable with available studies in the literature.

As seen from the literature survey, the researchers used both analytical and numerical methods to solve transient heat conduction and mass transfer problems. Most of the researchers used software that solved FDM of FVM methods. Some of the studies included their solutions by using a numerical approach. On the other hand, there are some software or GUI to solve transient heat conduction problems but they are limited to simple geometries.

In this study, a novel and user-friendly MATLAB2023b-based GUI is developed to solve transient heat and mass transfer in multidimensional solid objects by using exact solutions. Transient heat and mass transfer for infinite rectangular bars, finite cylinders, rectangular prisms, and spheres can be calculated. The application uses exact solutions to solve governing equations for multidimensional transient heat and mass transfer problems. Time-dependent temperature and moisture content in the objects can be displayed in graphs. Two- and three-dimensional temperature and moisture content contours are represented. The heat transfer at any time for heating or cooling processes can be found. Another important feature of the software is to find the time for the target temperature or moisture content, which is not available in previous studies.

2. Materials and Methods

The developed software is designed to solve transient heat conduction and diffusion mass transfer equations in Cartesian, cylindrical, and spherical coordinates. When thermal conductivity k, density ρ, and specific heat capacity c are assumed constant, without a heat generation term, these equations can be written as follows [36]:

$$\frac{\partial^2 T}{\partial x^2} + \frac{\partial^2 T}{\partial y^2} + \frac{\partial^2 T}{\partial z^2} = \frac{1}{\alpha}\frac{\partial T}{\partial t} \tag{1}$$

$$\frac{1}{r}\frac{\partial}{\partial r}\left(r\frac{\partial T}{\partial r}\right) + \frac{1}{r^2}\frac{\partial^2 T}{\partial \theta^2} + \frac{\partial^2 T}{\partial z^2} = \frac{1}{\alpha}\frac{\partial T}{\partial t} \tag{2}$$

$$\frac{1}{r^2}\frac{\partial}{\partial r}\left(r^2\frac{\partial T}{\partial r}\right) + \frac{1}{r^2 sin^2\theta}\frac{\partial^2 T}{\partial \emptyset^2} + \frac{1}{r^2 sin\theta}\frac{\partial}{\partial \theta}\left(sin\theta\frac{\partial T}{\partial \theta}\right) = \frac{1}{\alpha}\frac{\partial T}{\partial t} \tag{3}$$

In Equations (1)–(3), T is the temperature, t is the time, x, y, z, r, θ and $\emptyset$ are the spatial coordinates, and α is the thermal diffusivity which is $\alpha = k/\rho c$.

When the heat transfer in the z-direction in Equation (1) and the θ-direction in Equation (2) are neglected, the abovementioned equations are reduced into 2D and can be written as follows [36]:

$$\frac{\partial^2 T}{\partial x^2} + \frac{\partial^2 T}{\partial y^2} = \frac{1}{\alpha}\frac{\partial T}{\partial t} \tag{4}$$

$$\frac{1}{r}\frac{\partial}{\partial r}\left(r\frac{\partial T}{\partial r}\right) + \frac{\partial^2 T}{\partial z^2} = \frac{1}{\alpha}\frac{\partial T}{\partial t} \tag{5}$$

If only one-dimensional heat transfer is significant, the heat conduction equations are reduced to [1]:

$$\frac{\partial^2 T}{\partial x^2} = \frac{1}{\alpha}\frac{\partial T}{\partial t} \tag{6}$$

$$\frac{1}{r}\frac{\partial}{\partial r}\left(r\frac{\partial T}{\partial r}\right) = \frac{1}{\alpha}\frac{\partial T}{\partial t} \tag{7}$$

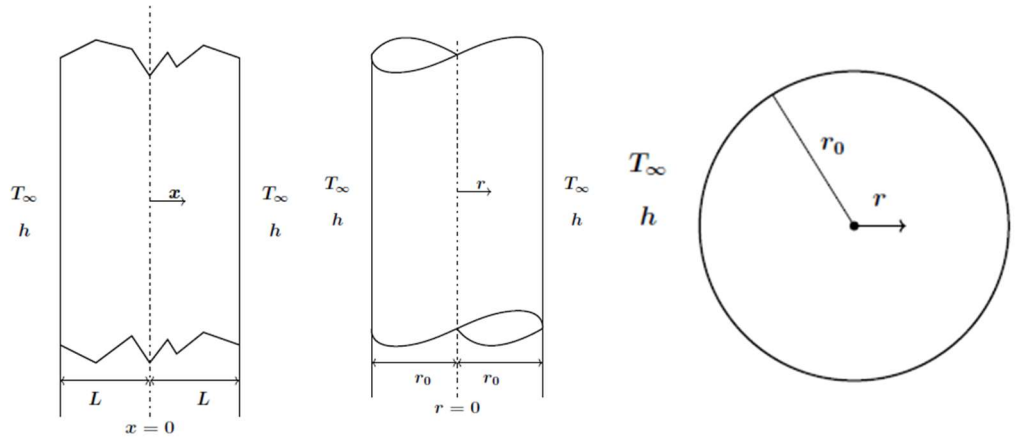
$$\frac{1}{r^2}\frac{\partial}{\partial r}\left(r^2\frac{\partial T}{\partial r}\right) = \frac{1}{\alpha}\frac{\partial T}{\partial t} \tag{8}$$

To solve Equation (6), a large plane wall with a thickness of 2 L is considered with heat convection on both sides. The problem can be presented in Figure 1a. When only the half of the system is considered, the boundary and initial conditions can be written as [1]:

$$\text{Boundary conditions: At } x = 0 \quad \frac{\partial T(0,t)}{\partial x} = 0$$

$$\text{At } x = L \quad -k\frac{\partial T(L,t)}{\partial x} = h[T(L,t) - T_\infty]$$

$$\text{Initial condition:} \quad T(x,0) = T_i$$



(**a**) (**b**) (**c**)

Figure 1. Plane wall with 2 L thickness (**a**), infinite cylinder with $2r_0$ diameter (**b**), and sphere with $2r_0$ diameter (**c**).

h is the convection heat transfer coefficient on the surface of the plane wall, T_∞ is the temperature of the fluid and T_i is the initial temperature. The exact solution of this problem is [37]:

$$\theta_{Plane\ wall} = \sum_{n=1}^{\infty} \frac{4sin\lambda_n}{2\lambda_n + \sin(2\lambda_n)} e^{-\lambda_n^2 Fo_L} \cos(\lambda_n x/L) \tag{9}$$

The discrete values of λ_n are positive roots and can be found numerically with the transcendental equation of:

$$\lambda_n tan\lambda_n = Bi_L \tag{10}$$

$$\theta_{Plane\ wall} = \frac{\theta}{\theta_i} = \frac{T(x,t)-T_\infty}{T_i-T_\infty} \qquad Bi_L = \frac{hL}{k} \qquad Fo_L = \frac{\alpha t}{L^2}$$

Bi_L and Fo_L are the Biot and Fourier numbers for the plane wall, respectively. These two dimensionless numbers should be calculated by using the half-length, *L*, of the problem.

To solve Equation (7), an infinite cylinder with a diameter of $2r_0$ is considered with heat convection on both sides. The problem can be presented in Figure 1b. When only the half of the system is considered, the boundary and initial conditions can be written as [1]:

$$\text{Boundary conditions: At } r = 0 \quad \frac{\partial T(0,t)}{\partial r} = 0$$

$$\text{At } r = r_0 \quad -k\frac{\partial T(r0,t)}{\partial r} = h[T(r_0,t) - T_\infty]$$

$$\text{Initial condition:} \quad T(r,0) = T_i$$

The exact solution of this problem is [37]:

$$\theta_{Infinite\ cylinder} = \sum_{n=1}^{\infty} \frac{2}{\lambda_n} \frac{J_1(\lambda_n)}{J_0^2(\lambda_n) + J_1^2(\lambda_n)} e^{-\lambda_n^2 Fo_C} J_0\,(\lambda_n r/r_0) \tag{11}$$

The roots for λ_n can be found with:

$$\lambda_n \frac{J_1(\lambda_n)}{J_0(\lambda_n)} = Bi_C \tag{12}$$

$$\theta_{Infinite\ cylinder} = \frac{\theta}{\theta_i} = \frac{T(r,t)-T_\infty}{T_i-T_\infty} \qquad Bi_C = \frac{hr_0}{k} \qquad Fo_C = \frac{\alpha t}{{r_0}^2}$$

Bi_C and Fo_C are the Biot and Fourier numbers for the infinite cylinder, respectively. These two dimensionless numbers should be calculated by using the radius, r_0, of the problem. J_0 and J_1 are the Bessel functions of the first kind with the order of zero and one, respectively.

To solve Equation (8), a sphere with a diameter of $2r_0$ is considered with heat convection on boundaries. The problem can be presented in Figure 1c. The boundary and initial conditions can be written as [1]:

$$\text{Boundary conditions: At } r = 0 \quad \frac{\partial T(0,t)}{\partial r} = 0$$

$$\text{At } r = r_0 \quad -k\frac{\partial T(r0,t)}{\partial r} = h[T(r_0,t) - T_\infty]$$

$$\text{Initial condition:} \quad T(r,0) = T_i$$

The exact solution of this problem is [37]:

$$\theta_{Sphere} = \sum_{n=1}^{\infty} \frac{4[sin\lambda_n - \lambda_n cos\lambda_n]}{2\lambda_n - sin2\lambda_n} e^{-\lambda_n^2 Fo_C} \frac{1}{\lambda_n r/r_0} \sin(\lambda_n r/r_0) \tag{13}$$

The roots for λ_n can be found with:

$$1 - \lambda_n cot\lambda_n = Bi_S \tag{14}$$

$$\theta_{Sphere} = \frac{\theta}{\theta_i} = \frac{T(r,t)-T_\infty}{T_i-T_\infty} \qquad Bi_S = \frac{hr_0}{k} \qquad Fo_S = \frac{\alpha t}{{r_0}^2}$$

Bi_S and Fo_S are the Biot and Fourier numbers for the sphere, respectively. These two dimensionless numbers should be calculated by using the radius, r_0, of the problem.

The amount of heat transfer rate during definite time of t can be calculated as [1]:

$$\frac{Q}{Q_{max}} = \frac{1}{\forall}\int (1-\theta)d\forall \tag{15}$$

where $\forall$ is the volume of the object and the maximum heat transfer rate can be found with:

$$Q_{max} = \rho \forall c(T_\infty - T_i) \tag{16}$$

$$\left(\frac{Q}{Q_{max}}\right)_{Plane\ wall} = 1 - \sum_{n=1}^{\infty} \frac{4sin\lambda_n}{2\lambda_n + sin\,(2\lambda_n)} \frac{sin\lambda_n}{\lambda_n} e^{-\lambda_n^2 Fo_L} \tag{17}$$

$$\left(\frac{Q}{Q_{max}}\right)_{Infinite\ cylinder} = 1 - \sum_{n=1}^{\infty} \frac{4}{\lambda_n} \frac{J_1(\lambda_n)}{J_0^2(\lambda_n) + J_1^2(\lambda_n)} \frac{J_1(\lambda_n)}{\lambda_n} e^{-\lambda_n^2 Fo_C} \tag{18}$$

$$\left(\frac{Q}{Q_{max}}\right)_{Sphere} = 1 - \sum_{n=1}^{\infty} 3\left[\frac{4[sin\lambda_n - \lambda_n cos\lambda_n]}{2\lambda_n - sin2\lambda_n}\right] \frac{sin\lambda_n - \lambda_n cos\lambda_n}{\lambda_n^3} e^{-\lambda_n^2 Fo_S} \tag{19}$$

For multidimensional heat conduction, the superposition approach called product solution can be used [1]. Product solutions of infinite rectangular bar, rectangular prism, and short cylinder are presented in Table 1.

For calculating the heat transfer rate of a multidimensional system a modified version of the product solution can be used as described by Langston [38]. The total transient heat transfer rate of two-dimensional geometry can be found by:

$$\left(\frac{Q}{Q_{max}}\right)_{Total\ 2-D} = \left(\frac{Q}{Q_{max}}\right)_1 + \left(\frac{Q}{Q_{max}}\right)_2 \left[1 - \left(\frac{Q}{Q_{max}}\right)_1\right] \tag{20}$$

Similarly, the total transient heat transfer rate of three-dimensional geometry can be found by:

$$\begin{aligned}\left(\frac{Q}{Q_{max}}\right)_{Total\ 3-D} &= \left(\frac{Q}{Q_{max}}\right)_1 + \left(\frac{Q}{Q_{max}}\right)_2 \left[1 - \left(\frac{Q}{Q_{max}}\right)_1\right] \\ &+ \left(\frac{Q}{Q_{max}}\right)_3 \left[1 - \left(\frac{Q}{Q_{max}}\right)_1\right]\left[1 - \left(\frac{Q}{Q_{max}}\right)_2\right]\end{aligned} \tag{21}$$

The convective heat transfer coefficient can be found by using empirical Nusselt correlations that are available in the literature. Nusselt correlations for different geometries that are used in the study are presented in Table 2.

The thermophysical properties of the fluid (k, ν, Pr) should be calculated at film temperature as $T_f = (T_\infty + T_s)/2$. Re is the Reynolds number which should be calculated by the appropriate length according to the flow geometry L and bulk velocity U as $Re = UD/\nu$ and h the heat transfer coefficient can be found with $Nu = hD/k$.

Table 1. Product solutions of infinite rectangular bar, rectangular prism, and short cylinder.

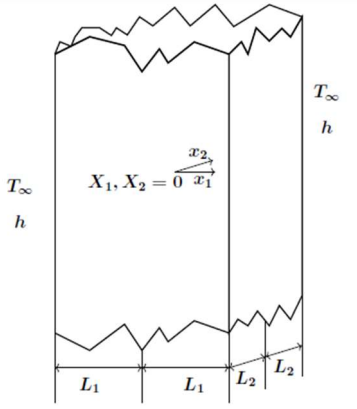
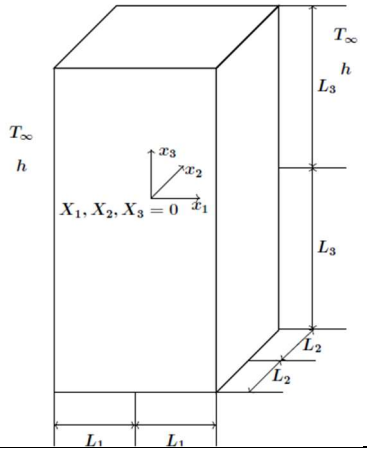
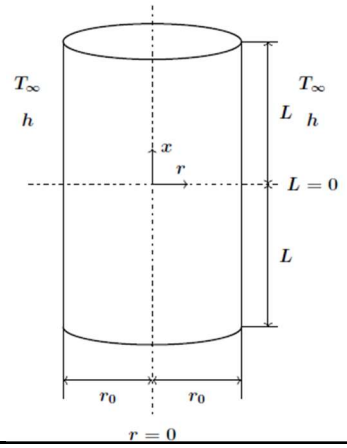
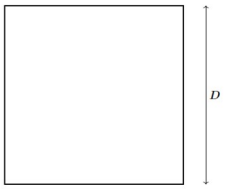
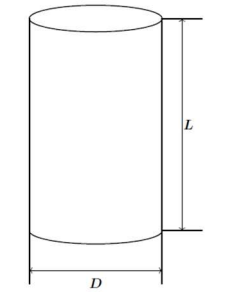
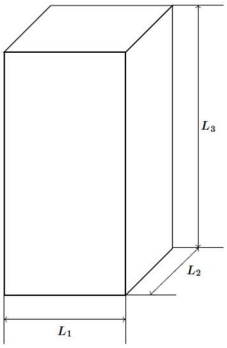
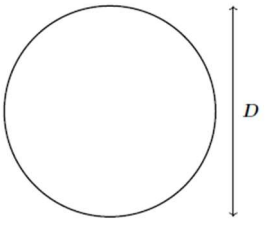
Infinite Rectangular Bar	Product Solution
	$\theta = \theta_{Plane\ wall\ I} x \theta_{Plane\ wall\ II}$
Rectangular Prism	
	$\theta = \theta_{Plane\ wall\ I} x \theta_{Plane\ wall\ II} x \theta_{Plane\ wall\ III}$
Short Cylinder	
	$\theta = \theta_{Plane\ wall\ I} x \theta_{Infinite\ Cylinder}$

Table 2. Convective heat transfer correlations for geometries.

Geometry	Nusselt Correlations
Flat Plate	$Nu = 0.664Re^{0.5}Pr^{1/3}$ [1] $5 \times 10^5 < Re, Pr > 0.6$ $Nu = 0.037Re^{0.8}Pr^{1/3}$ [1] $5 \times 10^5 < Re < 10^7, 0.6 \leq Pr \leq 60$
	$Nu = 0.094Re^{0.675}Pr^{1/3}$ [1] $3900 < Re < 79{,}000$
	$Nu = 0.683Re^{0.466}Pr^{1/3}$ $40 < Re < 4000$ $Nu = 0.193Re^{0.618}Pr^{\frac{1}{3}}$ [1] $4000 < Re < 40{,}000$ $Nu = 0.027Re^{0.805}Pr^{1/3}$ $40{,}000 < Re < 400{,}000$
	$Nu = (0.1037Re_{L_3}^{0.7158})(1.1 - 4.4L_2 + 4.3L_3 + 14.6L_3^2 - 7.4L_1 + 314.2L_1^2 - 2478L_1^3 - 0.004a)$ $13{,}300 < Re_{L_3} < 63{,}500$ a is the angle of attack [39]
	$Nu = 2 + \left[0.4Re^{1/2} + 0.06Re^{2/3}\right]Pr^{0.4}(\mu_\infty/\mu_s)^{1/4}$ [1]

Transient mass transfer for Cartesian, cylindrical, and spherical coordinates with moisture content M in one dimension can be written by taking constant density ρ and moisture diffusivity, D_m as [36]:

$$\frac{\partial^2 M}{\partial x^2} = \frac{1}{D_m}\frac{\partial M}{\partial t} \quad (22)$$

$$\frac{1}{r}\frac{\partial}{\partial r}\left(r\frac{\partial M}{\partial r}\right) = \frac{1}{D_m}\frac{\partial M}{\partial t} \quad (23)$$

$$\frac{1}{r^2}\frac{\partial}{\partial r}\left(r^2\frac{\partial M}{\partial r}\right) = \frac{1}{D_m}\frac{\partial M}{\partial t} \quad (24)$$

The boundary and initial conditions can be written to solve Equation (22) as [24]:

$$\text{Boundary conditions: At } x = 0 \quad \frac{\partial M(0,t)}{\partial x} = 0$$

$$\text{At x} = L \quad -D_m \frac{\partial M(L,t)}{\partial x} = h_m[M(L,t) - M_\infty]$$

$$\text{Initial condition:} \quad M(x,0) = M_i$$

The boundary and initial conditions for solving Equations (23) and (24) can be written as [40]:

$$\text{Boundary conditions: At } r = 0 \quad \frac{\partial M(0,t)}{\partial r} = 0$$

$$\text{At } r = r_0 \quad -D_m \frac{\partial M(r0,t)}{\partial r} = h_m[M(r_0,t) - M_\infty]$$

$$\text{Initial condition:} \quad M(r,0) = M_i$$

M_i is the initial moisture content and h_m is the mass transfer coefficient.

The exact solutions of Equations (22)–(24) are identical to the solutions for heat transfer equations that are given in Equations (9)–(13). There is just a slight difference in the definition of Bi_m and Fo_m numbers which are Biot and Fourier numbers for mass transfer [36].

$$\theta_{Plane\ wall,m} = \frac{\theta_m}{\theta_i} = \frac{M(x,t)-M_\infty}{M_i-M_\infty} \qquad Bi_{Lm} = \frac{h_m L}{D_m} \qquad Fo_{Lm} = \frac{D_m t}{L^2}$$

$$\theta_{Infinite\ cylinder,m} = \frac{\theta_m}{\theta_i} = \frac{M(r,t)-M_\infty}{M_i-M_\infty} \qquad Bi_{Cm} = \frac{h_m r_0}{D_m} \qquad Fo_{Cm} = \frac{D_m t}{{r_0}^2}$$

$$\theta_{Sphere,m} = \frac{\theta_m}{\theta_i} = \frac{M(r,t)-M_\infty}{M_i-M_\infty} \qquad Bi_{Sm} = \frac{h_m r_0}{D_m} \qquad Fo_{Sm} = \frac{D_m t}{{r_0}^2}$$

The mass transfer coefficient h_m can be found in [24]

$$h_m = h\left(\frac{D_m Le^{1/3}}{k_{fluid}}\right)$$

Le is the Lewis number.

$$Le = \frac{\alpha_{fluid}}{D_m}$$

The flowchart of the software for the calculation of final temperature or moisture content for a given time is presented in Figure 2. At the beginning of the application, the user chooses geometry and heat or mass transfer problems. Then, the user enters the material properties, heat or mass transfer coefficient values, the dimensions of the geometry, time, ambient, and initial conditions. The program calculates *Bi*, *Fo* numbers, and λ_n values for the chosen geometries. After calculating θ and Q/Q_{max} values, the product solution of the system is calculated. *Bi*, *Fo* numbers, θ, temperature or moisture content values, and heat transfer are displayed on the screen. Finally, graphics of temperature or moisture content variations with time, and temperature or moisture contours are displayed on the screen.

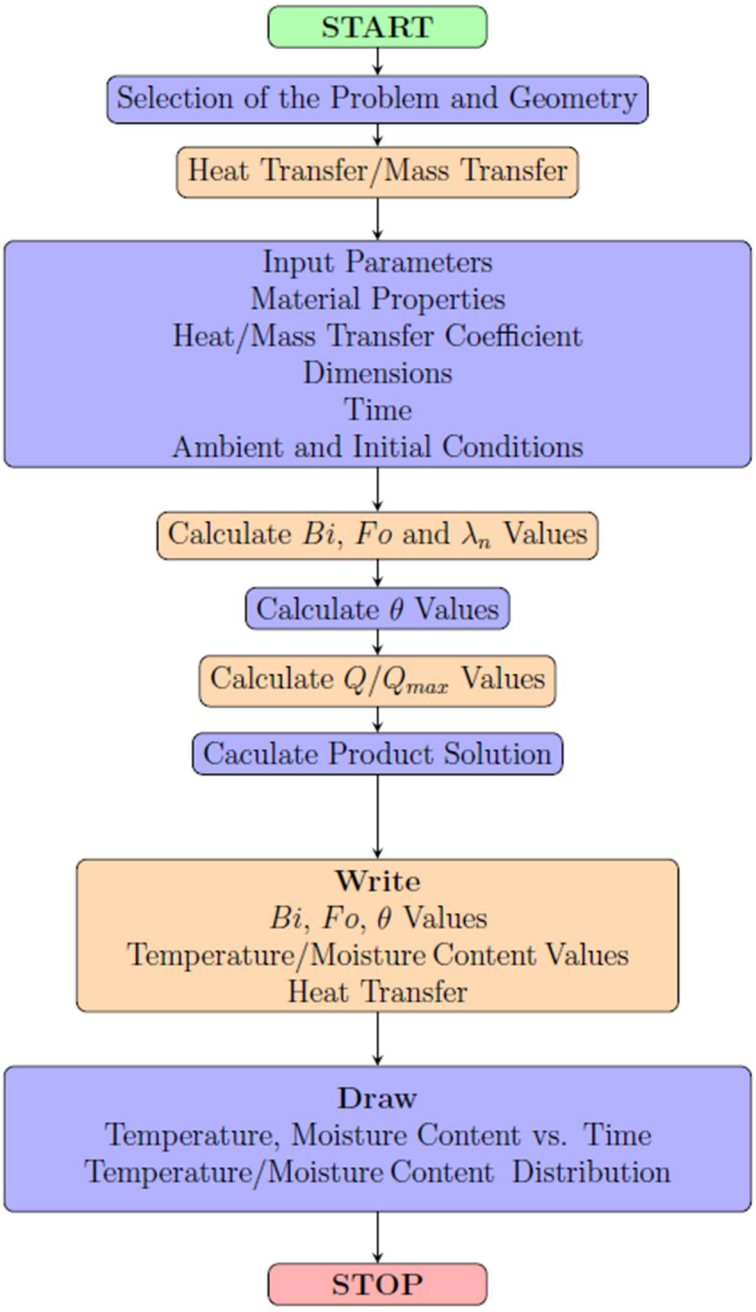


Figure 2. Flow diagram of temperature/mass content calculations.

In Figure 3, the flowchart to find the required time for a given specific temperature or moisture content is presented. After choosing the geometry and heat or mass transfer problem, the user enters the material properties, heat or mass transfer coefficients, dimensions, temperature or moisture content, and ambient and initial conditions. The software calculates θ, Bi and λ_n values. Then, time is calculated from product solutions and Bi, θ, temperature, or moisture content values and time are written on the screen. In all calculations, MATLAB 2023b is used.

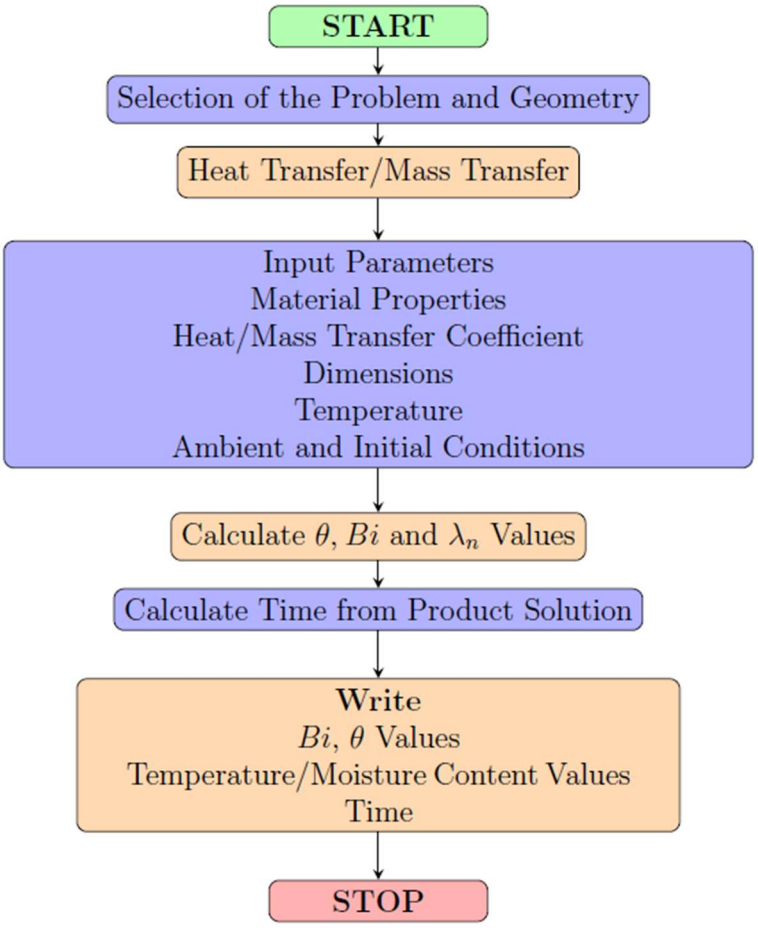


Figure 3. Flow diagram of time calculations.

3. Results

Validation of the Application

The validation of the software for transient heat transfer is calculated for an infinite rectangular bar, a rectangular prism, and a short cylinder. The infinite rectangular bar with a square cross-section has a side length of 0.3 m, initial temperature of 30 °C, ambient temperature of 750 °C, and a heat transfer coefficient of 100 W/m²K time to reach 600 °C central temperature [36]. For the problem with rectangular prism with dimensions of 0.06 m × 0.09 m × 0.2 m, the initial temperature of 1327 °C, ambient temperature of 40 °C, heat transfer coefficient of 50 W/m²K to find the central and corner temperature of the solid block after 50 min [36]. In the solution for the infinite rectangular bar and rectangular prism problems, the reference used Heisler charts. In the short cylinder problem that has a diameter of 0.08 m, a height of 0.15 m, an initial temperature of 150 °C, an ambient temperature of 20 °C, a heat transfer coefficient of 40 W/m²K to find the central, corner temperature, and heat transfer amount in 900 s was solved by using one-term approximation [1]. Freezing of a 9 cm diameter apple with 8 W/m²K heat transfer coefficient beginning from 20 °C with −15 °C air is compared with the one-term approach solution [1]. The results of the problems are compared in Table 3. As seen in Table 3, the software results are in good agreement with the references.

Table 3. Comparison of software results with references.

Geometry and Physical Conditions	Dimensions	Thermophysical Properties	Reference	Present Study
Infinite Rectangular Bar $T_{initial}$ = 30 °C T_∞ = 750 °C H = 100 W/m²K T_c = 600 °C	$L_1 = L_2$ = 0.3 m	ρ = 7854 kg/m³ c_p = 559 J/kgK k = 48 W/mK $\alpha = 1.093 \times 10^{-5}$ m²/s	6587 s [36]	6048 s
Rectangular Prism $T_{initial}$ = 1327 °C T_∞ = 40 °C h = 50 W/m²K t = 3000 s	L_1 = 0.06 m L_2 = 0.09 m L_3 = 0.2 m	ρ = 2050 kg/m³ c_p = 960 J/kgK k = 1 W/mK $\alpha = 0.51 \times 10^{-6}$ m²/s	T_c = 161 °C T_{corner} = 47 °C [36]	T_c = 161 °C T_{corner} = 48 °C
Short Cylinder $T_{initial}$ = 150 °C T_∞ = 20 °C h = 40 W/m²K t = 900 s	D = 8 cm L = 15 cm	ρ = 8530 kg/m³ c_p = 389 J/kgK k = 110 W/mK $\alpha = 3.39 \times 10^{-5}$ m²/s	T_c = 85.1 °C $T_{surface}$ = 84.2 °C Q = 164 kJ [1]	T_c = 85.1 °C $T_{surface}$ = 84.2 °C Q = 163.6 kJ
Sphere $T_{initial}$ = 20 °C T_∞ = −15 °C h = 8 W/m²K t = 3600 s	D = 9 cm	ρ = 840 kg/m³ c_p = 3810 J/kgK k = 0.418 W/mK $\alpha = 1.3 \times 10^{-7}$ m²/s	T_c = 11.2 °C $T_{surface}$ = 2.7 °C Q = 17.2 kJ [1]	T_c = 11.11 °C $T_{surface}$ = 2.67 °C Q = 17.216 kJ

The validation of mass transfer is calculated for square-cut apple slices with dimensions of 0.02 m × 0.02 m, initial moisture content of 7.196 kg/kg (db), moisture diffusivity of 1.7×10^{-9} m²/s, drying air moisture content of 0.196 kg/kg (db) and an average mass transfer coefficient of 9.12×10^{-3} m/s. The comparison of drying time with dimensionless moisture ϕ is presented in Figure 4. As seen in Figure 4, the drying time of the software is shorter. This is due to taking the mass transfer coefficient constant in calculations, whereas local mass transfer coefficient values were used in the reference study [41].

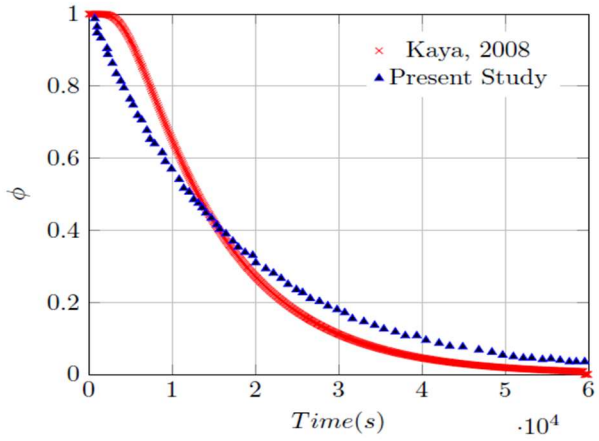


Figure 4. Comparison of dimensionless moisture variation with time [41].

The main screen of MULTITHMT is presented in Figure 5, where users can choose heat or mass transfer problems for desired geometries. The dimensionless numbers used in the software are described on the Dimensionless Numbers page. The users can get help

with the Help button, and for further assistance can reach the author of the manuscript by clicking the Contact button.

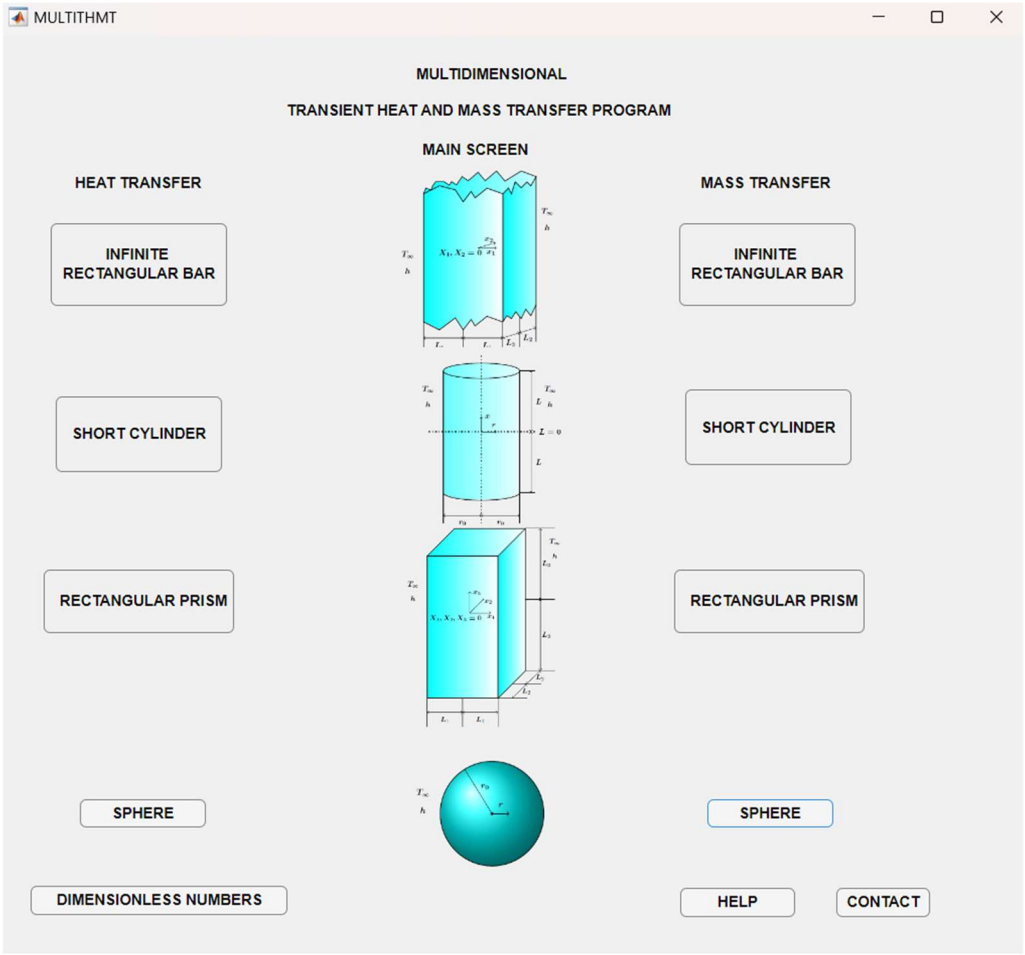


Figure 5. The main screen of the application.

3.1. Heat Transfer Calculations

The calculation of quenching of square-shaped (0.1 m × 0.1 m) AISI 1010 steel with V = 0.4 m/s water speed for initial temperature of 250 °C and water temperature of 25 °C for 300 s is presented in Figure 6. The user can see the instantaneous central, local temperature, and heat transfer rate by pointing to the desired time. Temperature contour for non-dimensional X_1 and X_2 directions are displayed on the upper right corner of the interface, where the user can display any temperature value at the final time of the calculation. Displayed graphs and contours can be saved and processed. The entire values of the calculation can be saved as a Microsoft Excel file with the Save button.

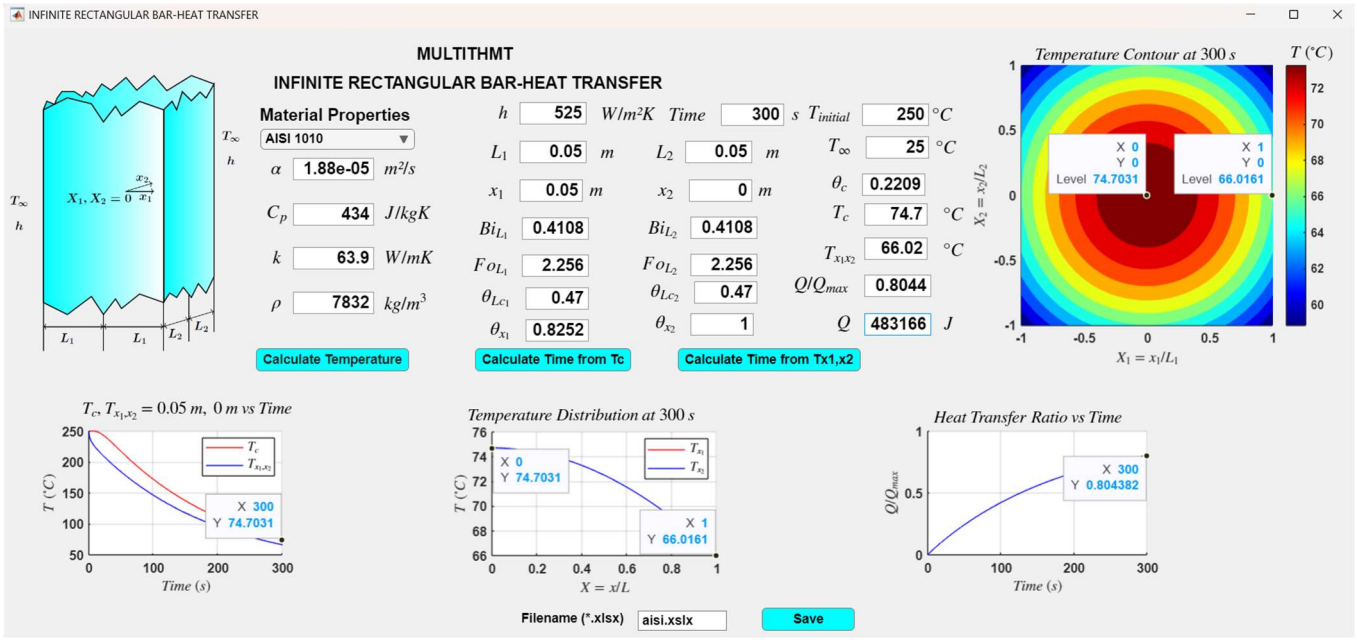


Figure 6. Cooling of AISI 1010 steel at V = 0.04 m/s.

Figure 7 represents the cooling period of AISI 1010 steel for V = 0.4–0.5–0.6 m/s water speed values. Since the heat transfer coefficient value of V = 0.6 m/s water speed has the highest value with 690 W/m²K the final temperature of this case is 58.3 °C. The heat transfer coefficient value of V = 0.5 m/s is 610 W/m²K and the final temperature is 65.28 °C. For the V = 0.4 m/s water speed case, the heat transfer coefficient is found as 525 W/m²K and the final temperature as 74.7 °C. The surface temperature variation with time can be seen in (b) where the values are 66.01 °C, 57.3 °C, and 51 °C, respectively, for increasing water speed values. Heat transfer ratio variation with time is represented in (c) as 0.8044, 0.8441, and 0.8731, respectively. Figure 8 represents the temperature contours of three cases at 300 s.

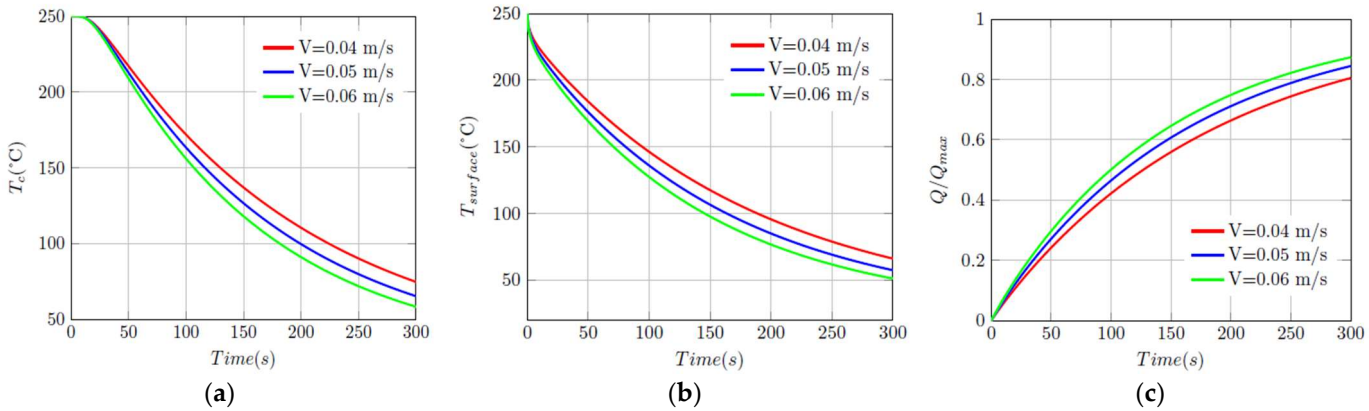


Figure 7. Central (**a**), surface (**b**) temperature, and heat transfer ratio (**c**) variation with time for cooling of AISI 1010 steel at V = 0.4–0.5–0.6 m/s.

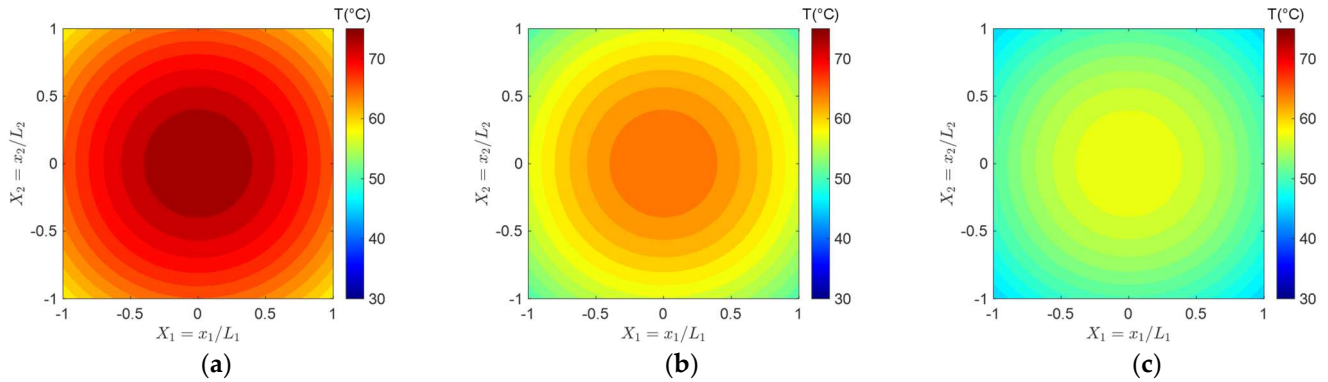


Figure 8. Temperature contours of AISI 1010 steel at 300 s, (**a**) V = 0.4 m/s, (**b**) V = 0.5 m/s and (**c**) V = 0.6 m/s.

Figure 9 represents the cooking of cylindirical shaped meat (α = 9.81 × 10^{-6} m^2/s, k = 0.45 W/m, c_p = 4100 J/kgK, ρ = 1200 kg/m^3) at 160 °C air temperature and 5 m/s air speed with initial temperature of 5 °C. The cylindrical meat dimensions are D = 0.07 m and L = 0.1 m. The total cooking time is 3600 s, and the final central temperature is 61.17 °C for cylindrical-shaped meat. According to the calculation, the heat transfer ratio after 3600 s is 0.6287 which yields 185 kJ. Temperature contours for non-dimensional geometry with 900 s interval are displayed in Figure 10.

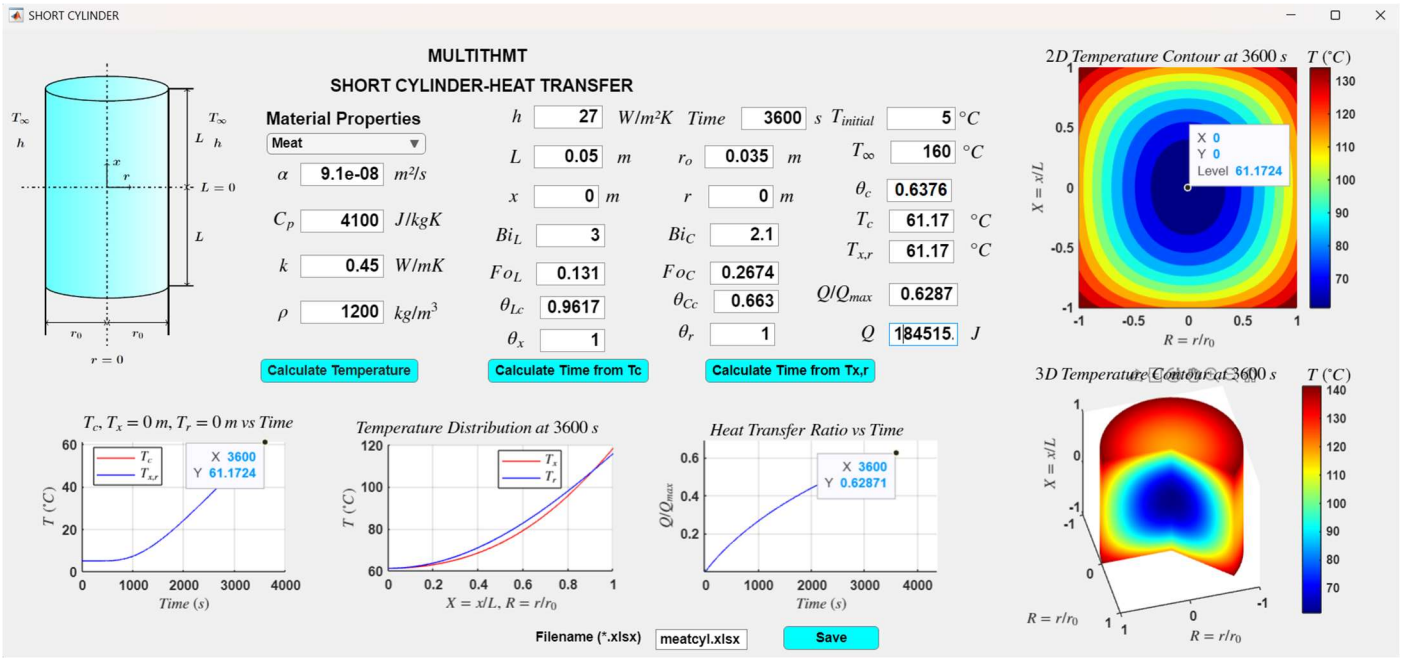


Figure 9. Cooking of cylindrical meat.

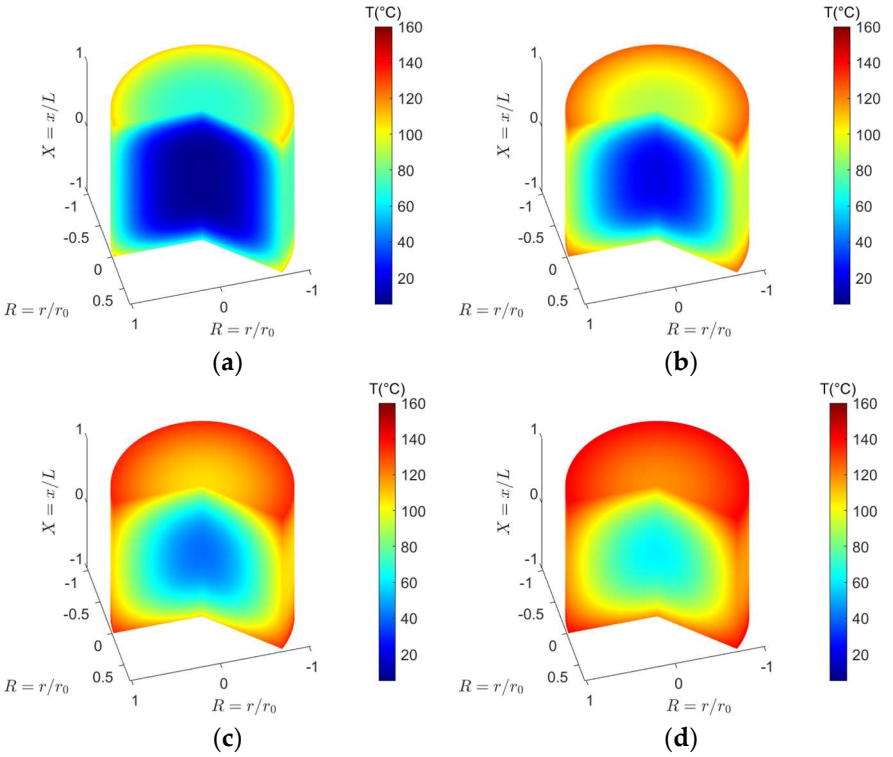


Figure 10. Cooking of cylindrical meat, (**a**) 900 s, (**b**) 1800 s, (**c**) 2700 s and (**d**) 3600 s.

The meat with a rectangular prism has the same height and volume as cylindrical meat where its dimensions are L_1 = 0.05 m, L_2 = 0.11 m, and L_3 = 0.07 m. The calculation for the rectangular prism-shaped meat is shown in Figure 11. The final temperature of the center is 76.57 °C. The heat transfer ratio for rectangular-shaped meat at the end of 3600 s cooking time is 0.7093, resulting in 208 kJ. Temperature contours of cooking for rectangular prism-shaped meat with 900 s intervals are presented in Figure 12.

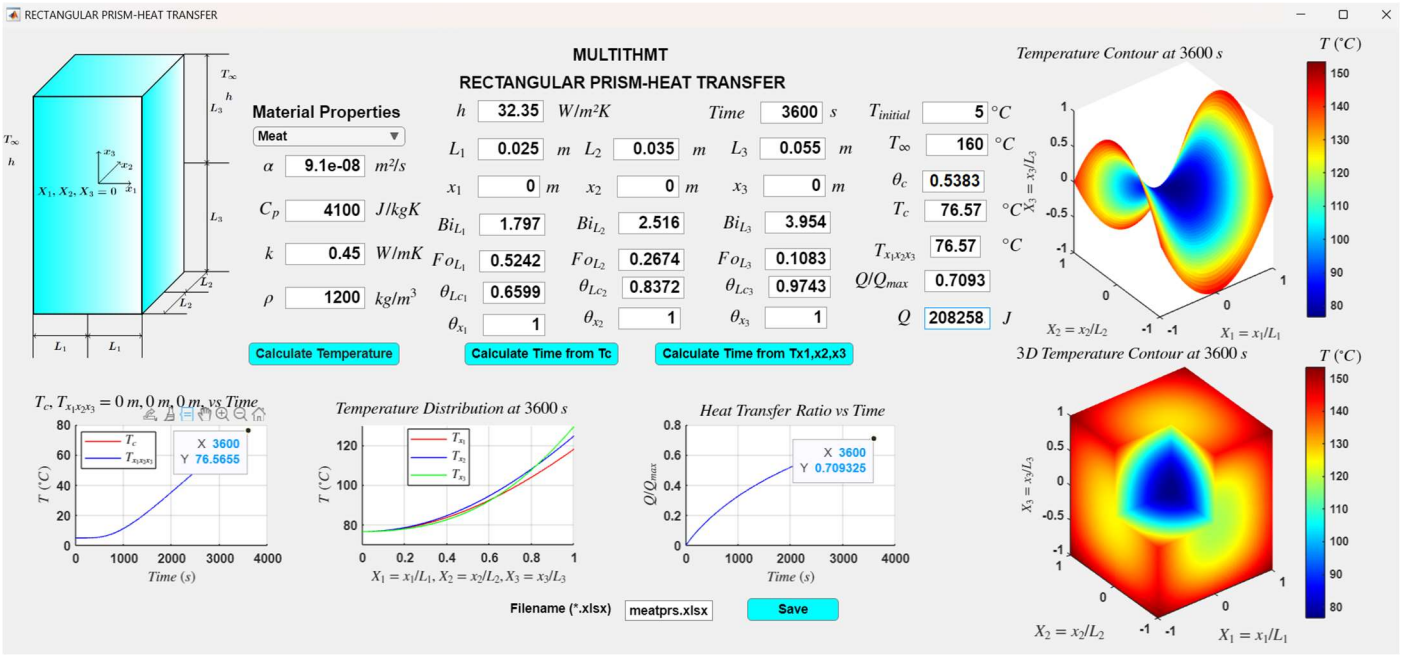


Figure 11. Cooking of meat with rectangular prism shape.

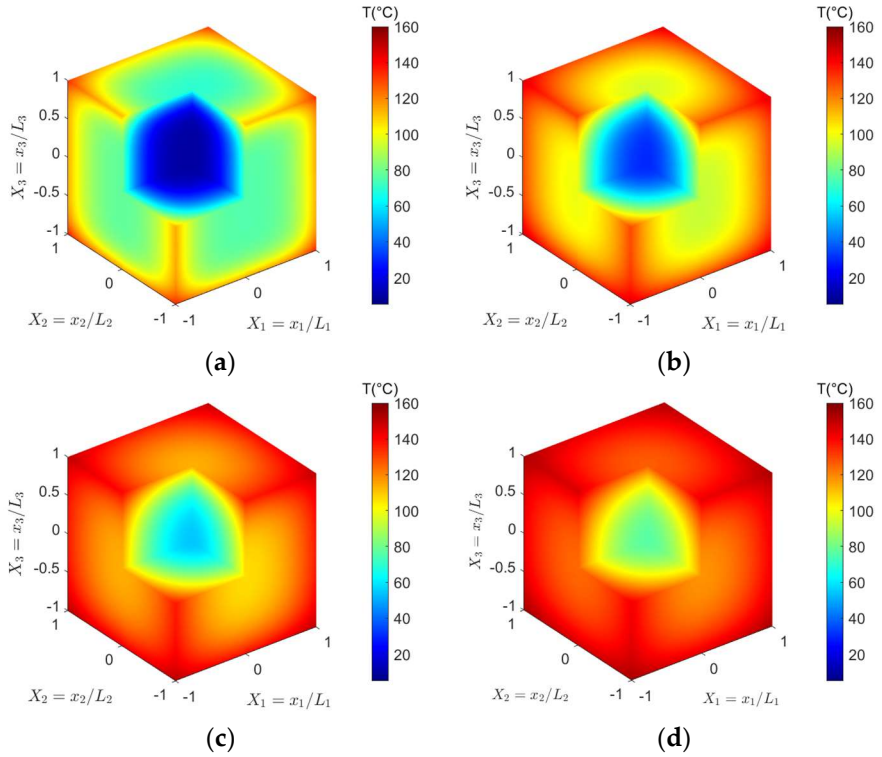


Figure 12. Cooking of rectangular prism meat, (**a**) 900 s, (**b**) 1800 s, (**c**) 2700 s and (**d**) 3600 s.

The comparison of the cooking process for the same volume of cylindrical and rectangular-shaped meat is given in Figure 13. As seen from the figure, the final central temperature and the heat transfer ratio of rectangular prism-shaped meat is higher than that of cylindrical shape. According to the calculations, heat transfer coefficients for these geometries are found as 32.25 W/m²K for the rectangular prism shape and 27 W/m²K for the cylindrical shape meat. If the central temperature of the meat is assumed to reach 60 °C for cooking time, it takes 2919 s to reach that target value for rectangular-shaped meat.

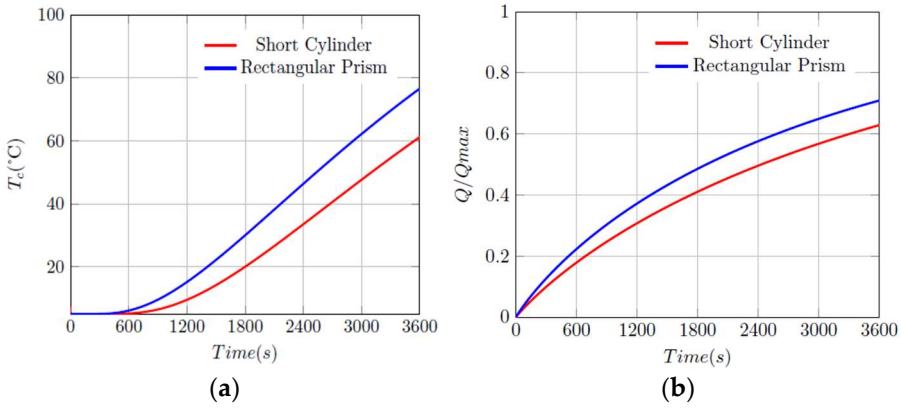


Figure 13. Cooking of meat for a short cylinder and rectangular prism, (**a**) Central temperature variation with time, (**b**) Heat transfer ratio variation with time.

For cooling of 0.1 m spherical iron and commercial bronze starting from an initial temperature of 200 °C with 25 °C water at 0.06 m/s water speed is considered. The heat transfer coefficient is found as 895 W/m²K. The cooling of the commercial bronze sphere is represented in Figure 14. The final temperature of the center point is calculated as 75.09 °C and the surface temperature is calculated as 58.8 °C. The heat transfer ratio during the cooling process is found as 0.7715 and heat transfer is found as 261 kJ.

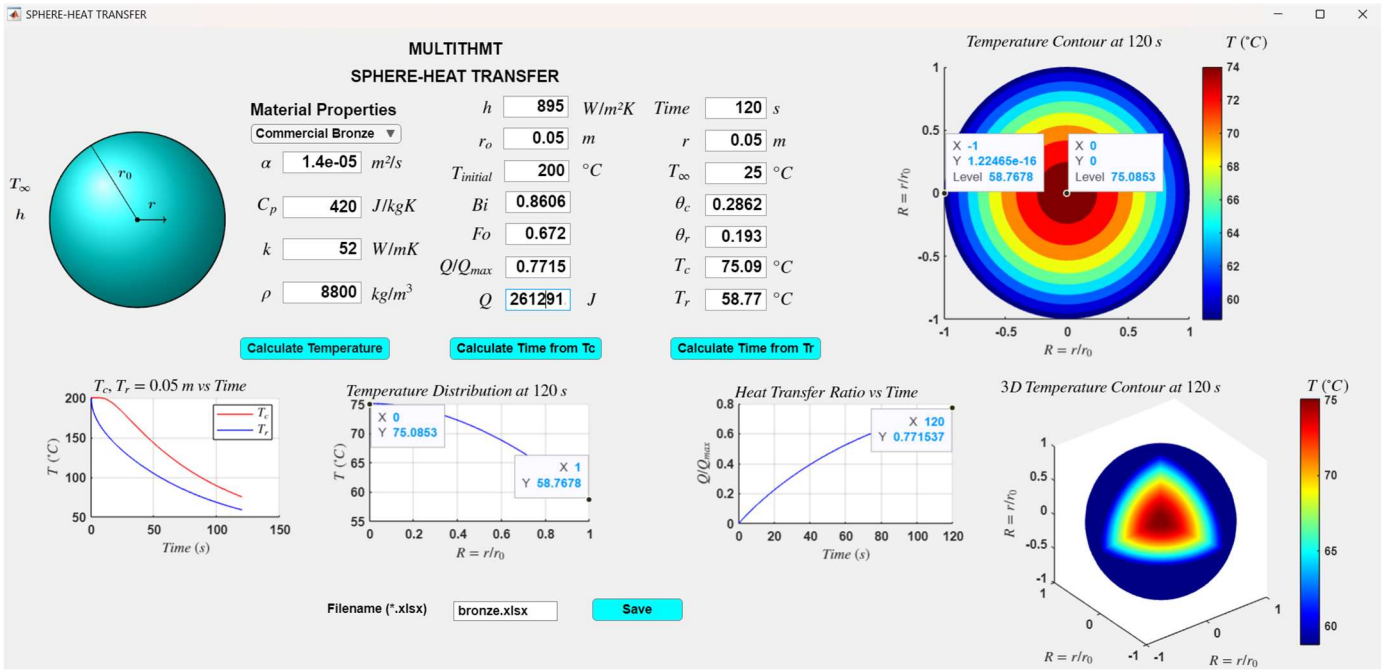


Figure 14. The cooling process of spherical commercial bronze.

The central and surface temperature variations with time during the cooling processes are compared in Figure 15a,b. The final central temperature values are found as 75.09 °C and 63.52 °C for commercial bronze and iron, respectively. The variations in the surface temperature values with time of the spherical commercial bronze and iron are almost the same. The final surface temperature values are found as 58.77 °C and 54.59 °C for commercial bronze and iron, respectively. The final heat transfer ratio values are found to be 0.7715 and 0.8112 for commercial bronze and iron, respectively. The heat transfer ratio of spherical commercial bronze and iron is presented in Figure 15c. Temperature contours of the cooling process with 30 s intervals are presented in Figure 16.

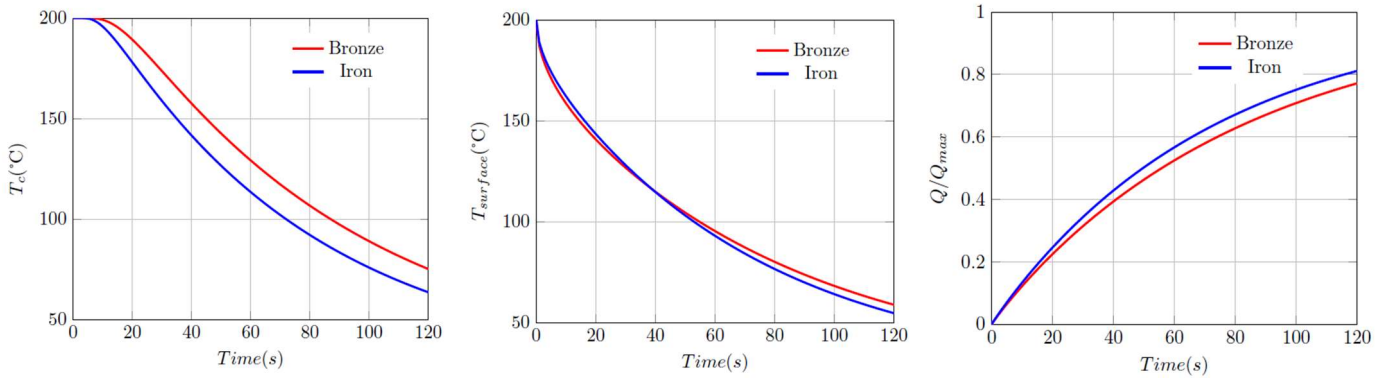


Figure 15. Central (**a**), surface (**b**) temperature, and heat transfer ratio (**c**) variation with time for cooling processes of spherical commercial and iron bronze.

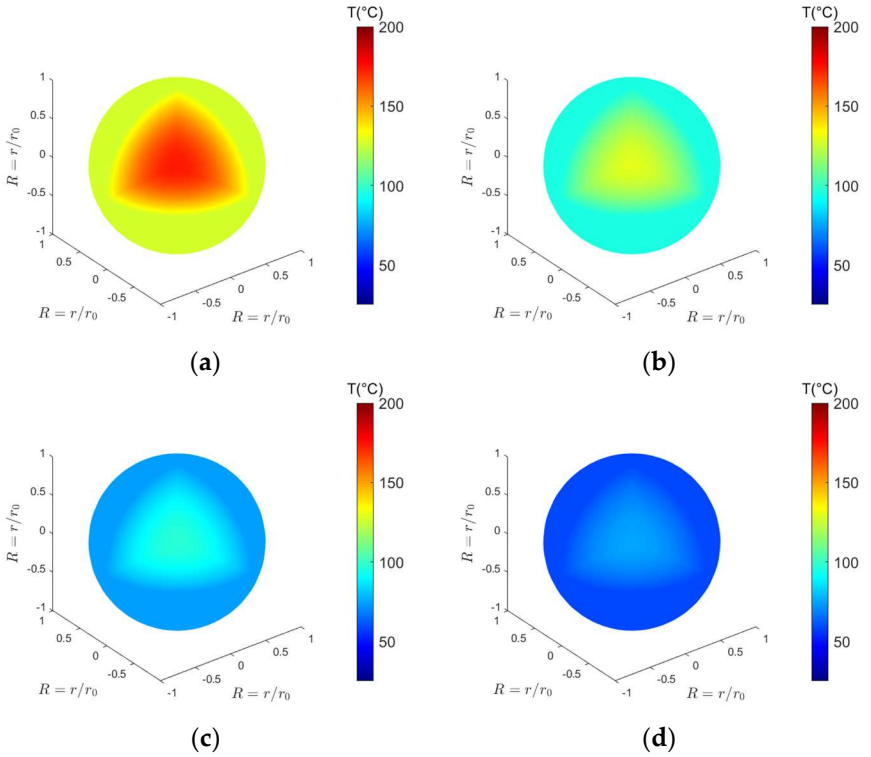


Figure 16. Cooling of spherical commercial bronze, (**a**) 30 s, (**b**) 60 s, (**c**) 90 s and (**d**) 120 s.

3.2. Mass Transfer Calculations

Convective drying of rectangular prunes with hot air for different aspect ratios is investigated. Air temperature is 80 °C and air velocity is 5 m/s. The initial moisture content of the prunes is taken as 0.7 kg/kg db whereas drying air moisture content is taken as 0.1 kg/kg db. The moisture diffusivity of prunes is taken as 7.64×10^{-9} m²/s [25]. The aspect ratios are taken as AR = 0.6–0.8–1 for rectangular prunes. The drying of rectangular prunes with AR = 0.6 is represented in Figure 17. The central moisture content is calculated at 36,000 s as 0.2174 kg/kg db.

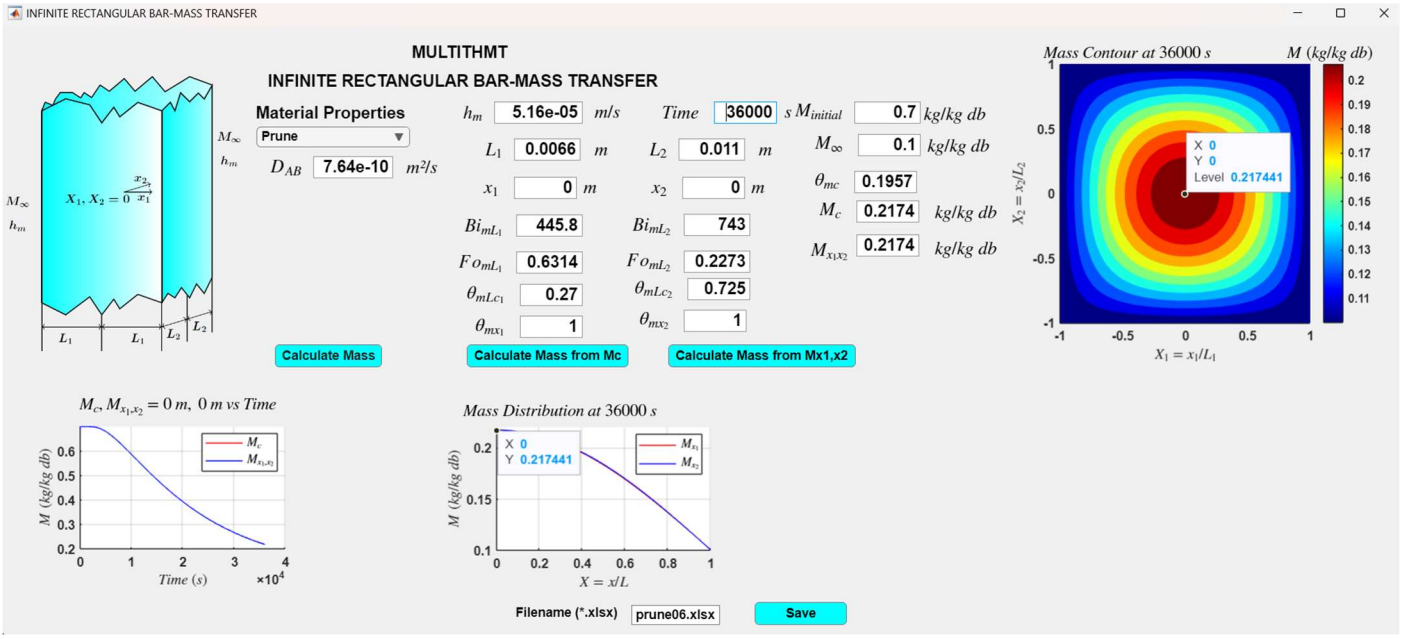


Figure 17. Convective drying of rectangular prunes with AR = 0.6.

Figure 18 shows the comparison of convective drying of prunes for AR = 0.6–0.8–1. The target dimensionless moisture content of the prunes is chosen as 0.2 for the end of the drying process. The overall drying times are 35,629 s, 52,566 s, and 67,334 s for AR = 0.6–0.8–1, respectively. Since the length of the rectangles is kept constant, the width of the prunes determines the aspect ratio. The mass transfer coefficient values for all aspect ratios are constant, therefore area of the prunes increases with increasing aspect ratio values, and a longer overall drying time is needed. In Figure 19, dimensionless moisture contours of the rectangular prunes at 5%, 10%, 20%, and 95% of the drying time for AR = 1 are represented.

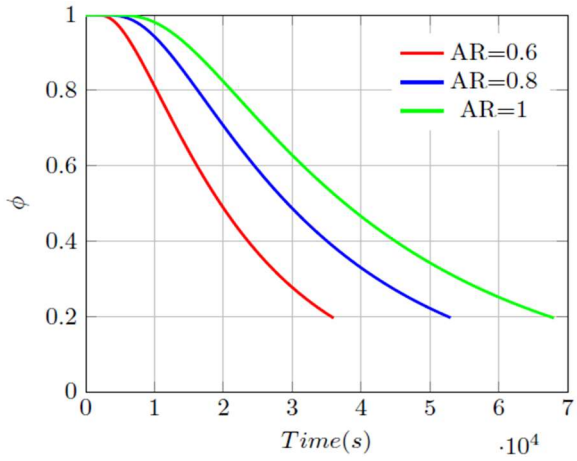


Figure 18. Convective drying of prunes with AR = 0.6–0.8–1.

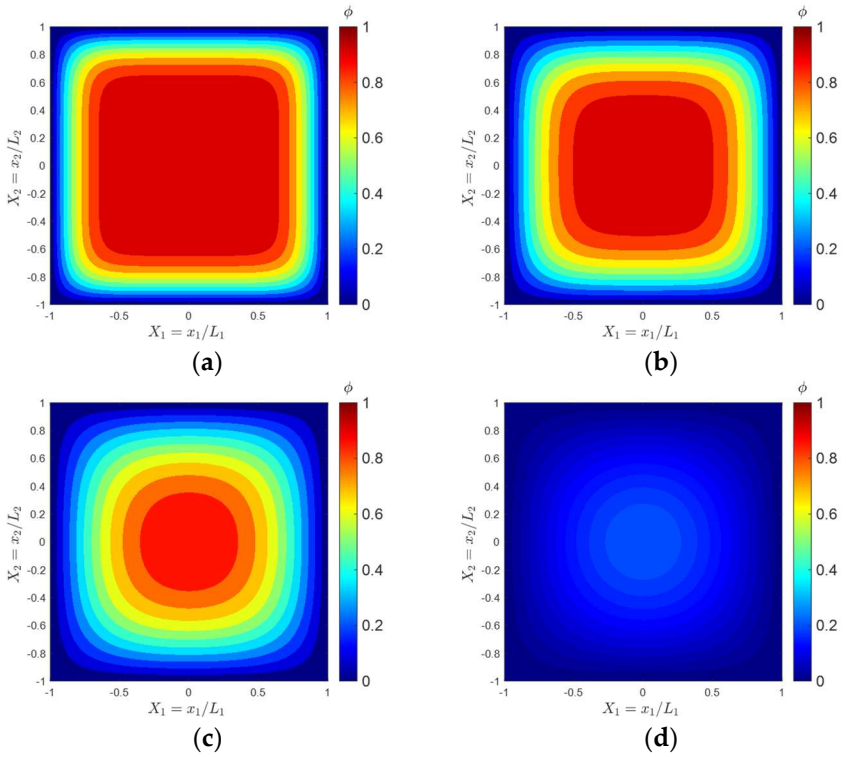


Figure 19. Dimensionless moisture contours of rectangular prunes for AR = 1, (**a**) 5% drying time, (**b**) 10% drying time, (**c**) 20% drying time, and (**d**) 95% drying time.

Bananas are another favorite drying fruit in the food industry. Convective drying or cylindrical bananas with hot air are studied for different drying air temperature values. The diameter of the bananas is 0.028 m and the height is 0.14 m. The drying parameters

for bananas are given in Table 4. Figure 20 shows the convective drying of cylindrical bananas for Case 1. As seen in Figure 20, the central moisture content in the banana is calculated as 0.2981 kg/kg db, and the moisture content on the banana surface is obtained as 0.1936 kg/kg db at 150,000 s. Figure 21 shows the dimensionless moisture value of banana drying cases with time. The overall drying times are calculated as 145,349 s, 125,975 s, and 101,646 s for Cases 1, 2 and 3, respectively. Dimensionless moisture contours of bananas at 5%, 10%, 20%, and 95% of the drying time for Case 1 are presented in Figure 22.

Table 4. Convective drying parameters for bananas [42].

Case	D_m (m²/s)	h_m (m/s)	M_i (kg/kg db)	M_∞ (kg/kg db)
Case I	1.86×10^{-9}	1.79×10^{-7}	3.21	0.0579
Case II	1.85×10^{-9}	2.48×10^{-7}	2.96	0.0426
Case III	2.97×10^{-9}	2.64×10^{-7}	2.95	0.0121

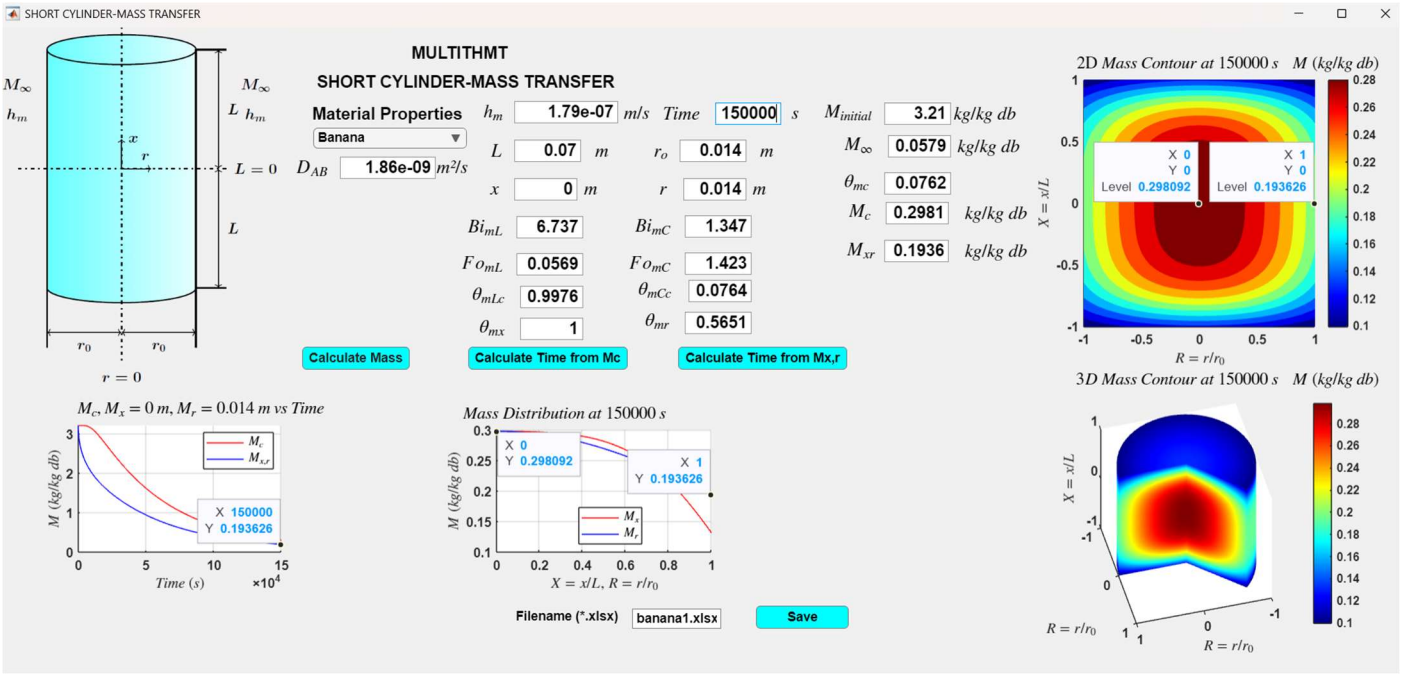


Figure 20. Convective drying of cylindrical banana for Case 1.

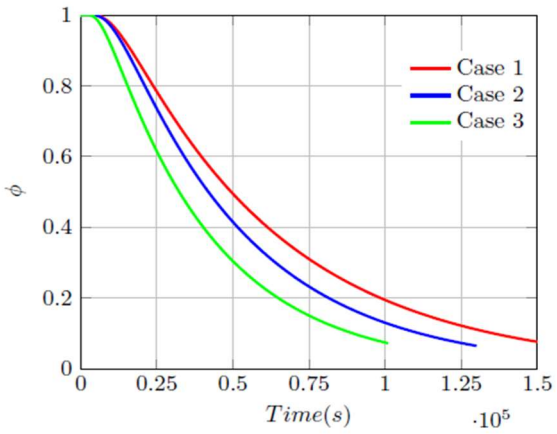


Figure 21. Convective drying of bananas for Cases 1–2 and 3.

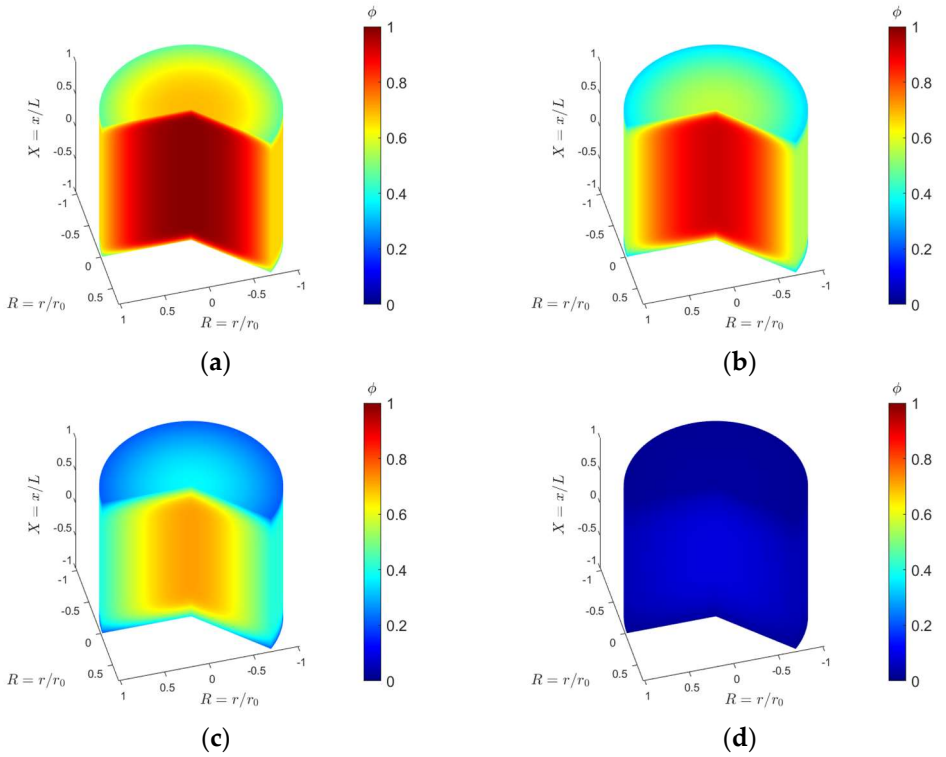


Figure 22. Dimensionless moisture contours of bananas. (**a**) 5% drying time, (**b**) 10% drying time, (**c**) 20% drying time, and (**d**) 95% drying time.

Convective drying of cubes with 0.04 m edge length at 40 °C air with Re = 200 for 1 × 10^{-5}, 1 × 10^{-6}, 1 × 10^{-7}, and 1 × 10^{-8} m^2/s moisture diffusivity values is investigated. The initial moisture content of the cubes is taken as 3 kg/kg db and the drying air moisture content is taken as 0.1 kg/kg db. The Nusselt number for Re = 200 is taken as 6.95 from the study of Mousazadeh [43]. According to Nu = 6.95, for 1 × 10^{-5}, 1 × 10^{-6}, 1 × 10^{-7} and 1 × 10^{-8} m^2/s moisture diffusivity values are found as 0.0048, 0.001, 2.2152 × 10^{-4} and 4.7725 × 10^{-5} m/s, respectively. Figure 23 shows the convective drying of cubes with 1 × 10^{-5} m^2/s moisture diffusivity. Time variation of dimensionless moisture content in the cubes for 1 × 10^{-5}, 1 × 10^{-6}, 1 × 10^{-7}, and 1 × 10^{-8} m^2/s moisture diffusivity values is presented in Figure 24. The overall drying times are calculated as 72, 644, 6200, and 60,653 s for 1 × 10^{-5}, 1 × 10^{-6}, 1 × 10^{-7}, and 1 × 10^{-8} m^2/s moisture diffusivity values, respectively. Dimensionless moisture contours of 1 × 10^{-5} m^2/s moisture diffusivity for 5%, 10%, 20%, and 95% drying time are presented in Figure 25.

The drying of cornelian cherries with D = 0.0114 m diameter at different air temperature values is investigated. The moisture diffusivity and mass transfer coefficient are obtained from [44]. The airspeed is kept at 0.7 m/s and the air temperature is changed from 50 °C–70 °C with 10 °C intervals. The initial moisture content of the cherries is taken as 3.065 kg/kg db and the moisture content of drying air is taken as 0.1 kg/kg db Table 5 represents the moisture diffusivity and the mass transfer coefficient values for the studied operating conditions. The drying process of the cherry at 50 °C is presented in Figure 26. As seen from the figure, the final moisture content is found as 0.11 kg/kg db. The moisture content on the cherry surface at the final state is found as 0.1063 kg/kg db.

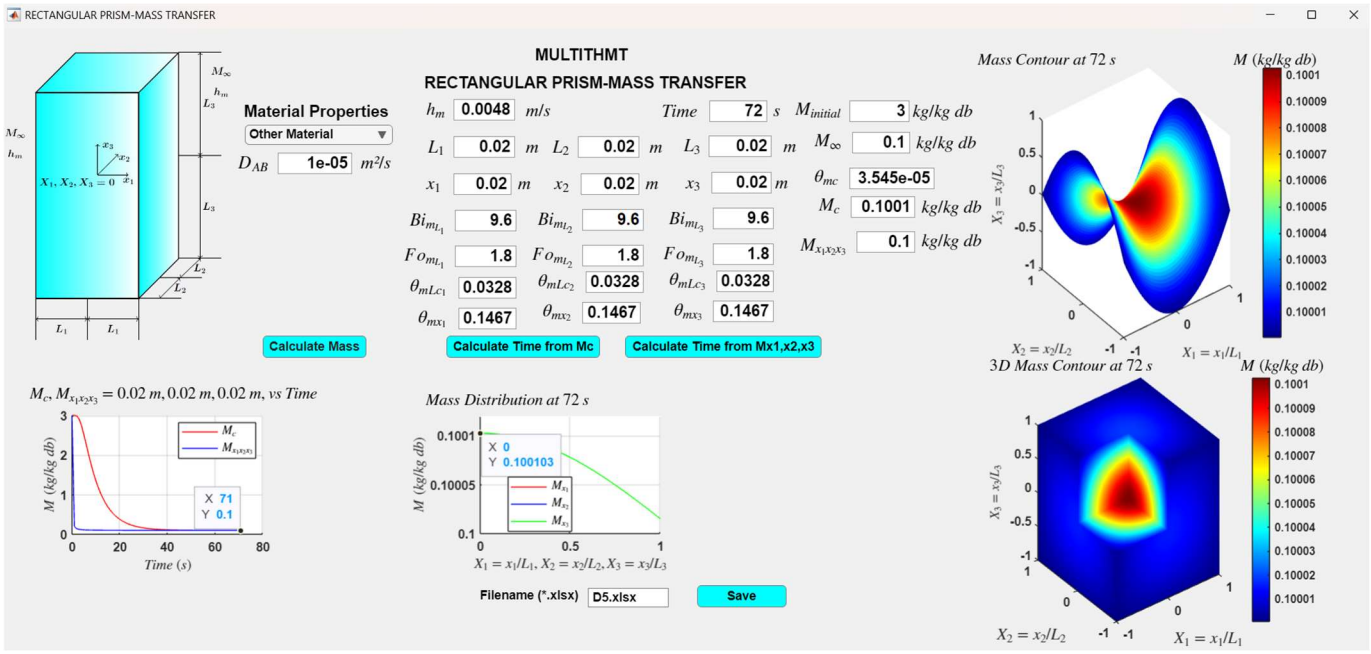


Figure 23. Convective drying of a cube for $D_m = 1 \times 10^{-5}$ m²/s.

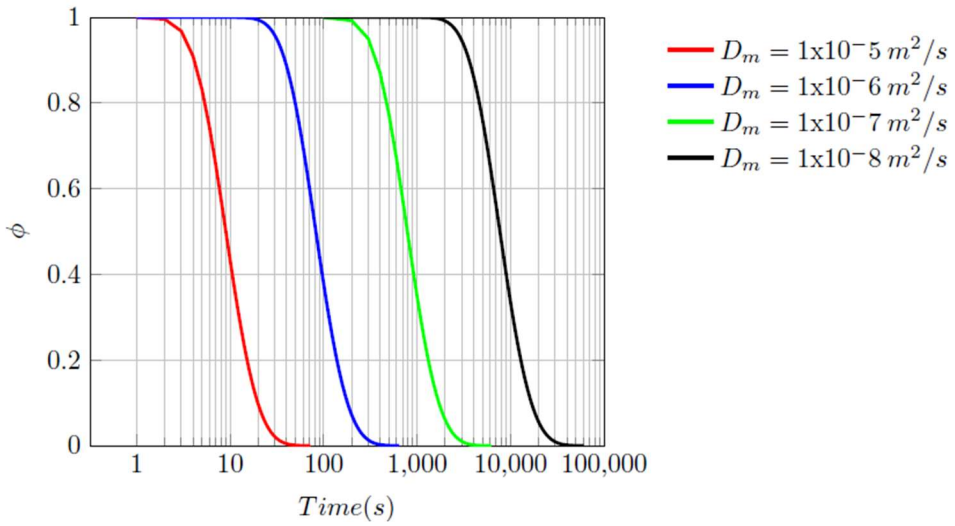
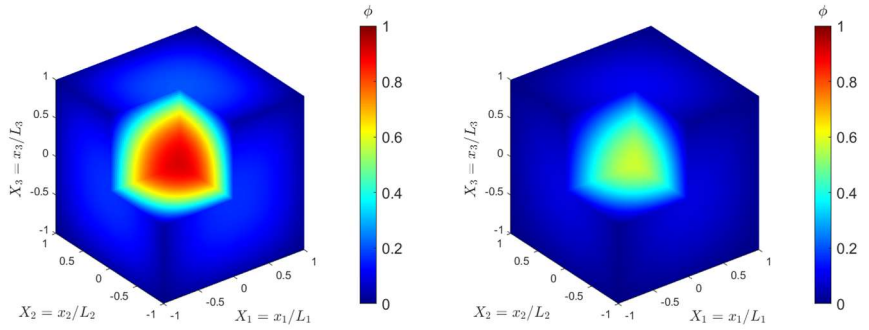
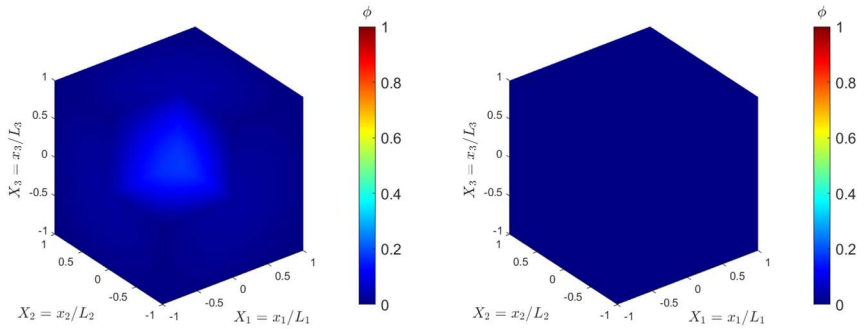


Figure 24. Dimensionless moisture variation of cubes with time for $D_m = 1 \times 10^{-5}$, 1×10^{-6}, 1×10^{-7}, and 1×10^{-8} m²/s.



(**a**) (**b**)



(**c**) (**d**)

Figure 25. Dimensionless moisture contours of cubes for D_m = 1 × 10^{-5} m^2/s: (**a**) 5% drying time, (**b**) 10% drying time, (**c**) 20% drying time, and (**d**) 95% drying time.

The comparison of drying times for the studied air temperature values is given in Figure 27. The overall drying times for 50 °C, 60 °C, and 70 °C air temperature values are 205,378 s, 104,182 s, and 51,191 s, respectively. The dimensionless moisture content contours for the drying process of cornelian cherry at 50 °C air temperature for 5%, 10%, 20%, and 95% of the drying time are represented in Figure 28.

Table 5. Convective drying parameters for cornelian cherries [44].

Air Temperature	D_m (m^2/s)	h_m (m/s)
50 °C	3.704 × 10^{-10}	6.726 × 10^{-8}
60 °C	9.648 × 10^{-10}	12.383 × 10^{-8}
70 °C	26.636 × 10^{-10}	23.945 × 10^{-8}

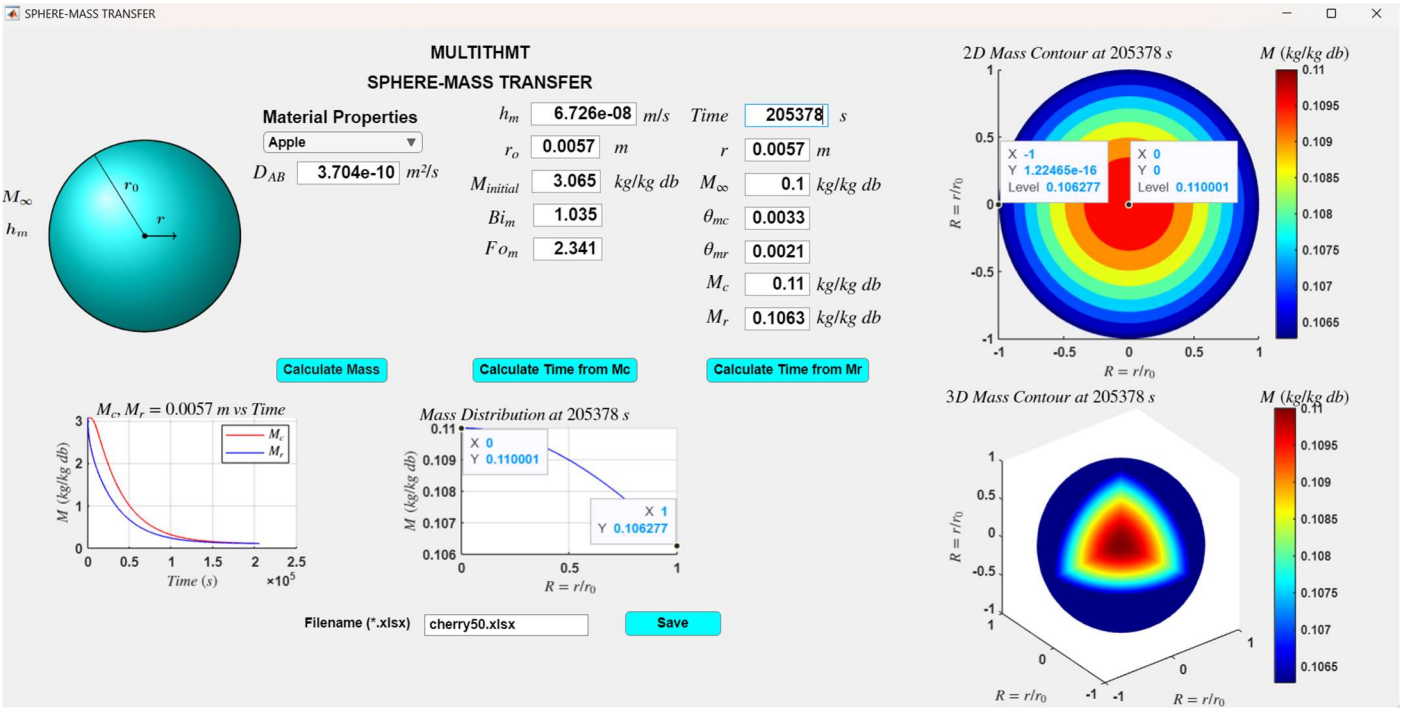


Figure 26. Convective drying of a cherry at 50 °C air temperature and 0.7 m/s airspeed.

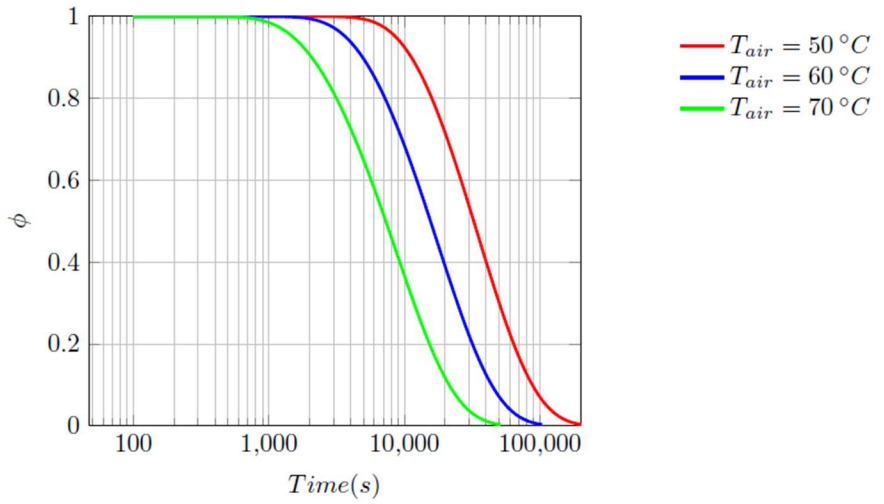


Figure 27. Dimensionless moisture variation of cherries with time for T_{air} = 50, 60, and 70 °C.

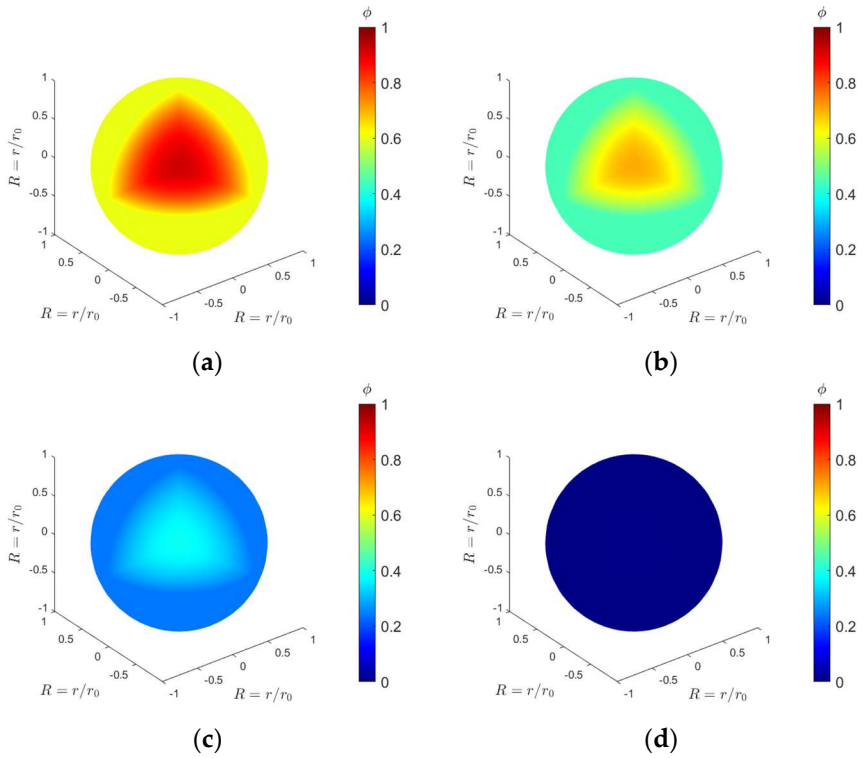


Figure 28. Dimensionless moisture contours of cherries for T_{air} = 50 °C. (**a**) 5% drying time, (**b**) 10% drying time, (**c**) 20% drying time, and (**d**) 95% drying time.

4. Conclusions

An interactive MATLAB application (MULTITHMT) has been created to address multidimensional transient heat and mass processes in a novel and user-friendly manner. This software utilizes exact solutions for transient heat conduction problems, allowing for the solution and visualization of transient heat conduction and diffusion mass transfer problems in infinite rectangular bars, short cylinders, rectangular prisms, and spheres. What sets this application apart is its ability to handle both of these problems within a single interface, which is not found in any other existing application. Additionally, this software offers a unique feature of determining the time required to reach a specific target temperature or moisture content.

The investigation delved into heat transfer issues, specifically exploring the quenching process of steel at varying velocities and the cooking of meat with different geometrical configurations. The cooling process of spherical commercial bronze and iron is studied, as well. The central temperature and heat transfer variation with time are presented. Two- and three-dimensional temperature contours of objects are presented.

For mass transfer, convective air drying of prunes with different aspect ratios, bananas and spherical Cornelian cherries with different operating conditions, and cubes with different moisture diffusivities were investigated. The central dimensionless moisture content variation with time and three-dimensional dimensionless moisture contours of the dried objects are presented.

This software is suitable for educational use across various engineering departments that cover topics related to transient heat and mass transfer. By utilizing this tool, students can enhance their understanding of these subjects. Moreover, the software offers a multitude of applications in industrial settings, particularly in processes that entail time-dependent heat and mass transfer. In future work, time-dependent thermophysical properties, constant temperature, constant heat flux, radiative boundary conditions for high-temperature differences, and a convection heat transfer library are planned to be added to the software.

Funding: This research received no external funding.

Data Availability Statement: The original contributions presented in the study are included in the article, further inquiries can be directed to the author.

Conflicts of Interest: The author declares no conflicts of interest.

Nomenclature

Bi	Biot number
cp	Specific heat capacity at constant pressure (J/kgK)
D	Diameter (m)
D_m	Moisture diffusivity (m^2/s)
Fo	Fourier number
h	Heat transfer coefficient (W/m^2K)
h_m	Mass transfer coefficient (m/s)
H	Height (m)
J	Bessel function
k	Thermal conductivity (W/mK)
L	Length (m)
Le	Lewis number
M	Mass (kg)
Q	Heat transfer (J)
r	Radius (m)
R	Dimensionless radius (r_0/r)
t	Time (s)
T	Temperature (°C)
x, y, z	Spatial coordinates (m)
V	Velocity (m/s)
$\forall$	Volume (m^3)
X	Dimensionless location (x/L)
Greek Letters	
α	Thermal diffusivity (m^2/s)
ϕ	Dimensionless moisture content
λ_n	Positive roots of the transcendental equation
ρ	Density (kg/m^3)
θ	Dimensionless temperature
Abbreviations	
AR	Aspect ratio
m	Mass

ι	Initial
∞	Ambient

References

1. Cengel, Y.A.; Ghajar, A.J. *Heat and Mass Transfer, Fundamentals&Applications*, 5th ed.; McGraw Hill Education: New York, NY, USA, 2015.
2. Hahn, D.W.; Özışık, M.N. *Heat Conduction*, 3rd ed.; Wiley: Hoboken, NJ, USA, 2002; Volume 5.
3. Heisler, M.P. Temperature Charts for Induction and Constant-Temperature Heating. *J. Fluids Eng. Trans. ASME* **1947**, *69*, 227–236. https://doi.org/10.1115/1.4017360.
4. Bird, R.B.; Stewart, W.E.; Lightfoot, E.N. *Transport Phenomena*, 2nd ed.; Wiley: Hoboken, NJ, USA, 1980; Volume 36.
5. Ibrahim, A.; Jiang, F. The electric vehicle energy management: An overview of the energy system and related modeling and simulation. *Renew. Sustain. Energy Rev.* **2021**, *144*, 111049. https://doi.org/10.1016/j.rser.2021.111049.
6. Baughn, J.W.; Rossi, M. Two-Dimensional transient heat conduction analysis using spreadsheets. *Heat Transf. Eng.* **1992**, *13*, 71–79. https://doi.org/10.1080/01457639208939775.
7. Yovanovich, M.M. Simple explicit expressions for calculation of the heisler-grober charts. In Proceedings of the 1996 Guidance, Navigation, and Control Conference and Exhibit, Monterey, CA, USA, 5–8 August 1996; pp. 1–9. https://doi.org/10.2514/6.1996-3968.
8. McMasters, R.L.; Dowding, K.J.; Beck, J.V.; Yen, D.H.Y. Methodology to generate accurate solutions for verification in transient three-dimensional heat conduction. *Numer. Heat Transf. Part B Fundam.* **2002**, *41*, 521–541. https://doi.org/10.1080/10407790190053761.
9. Antar, M.A.; Mokheimer, E.M. Spreadsheet modelling of transient three dimensional heat conduction with various standard boundary conditions. *Int. J. Mech. Eng. Educ.* **2002**, *30*, 17–34. https://doi.org/10.7227/IJMEE.30.1.3.
10. Zheng, H.; Keith, J.M. JAVA-based heat transfer visualization tools. *Chem. Eng. Educ.* **2004**, *38*, 282–285.
11. Ayatollahi, S.; Tauseef, S.M.; Guzman, C.; Mohebinia, S. Development of a user-friendly virtual laboratory for simulating three-dimensional transient heat transfer in regularly shaped solids. *Int. J. Mech. Eng. Educ.* **2008**, *36*, 81–89. https://doi.org/10.7227/IJMEE.36.1.9.
12. Li, Q.H.; Chen, S.S.; Kou, G.X. Transient heat conduction analysis using the MLPG method and modified precise time step integration method. *J. Comput. Phys.* **2011**, *230*, 2736–2750. https://doi.org/10.1016/j.jcp.2011.01.019.
13. Yang, K.; Jiang, G.H.; Li, H.Y.; Zhang, Z.B.; Gao, X.W. Element differential method for solving transient heat conduction problems. *Int. J. Heat Mass Transf.* **2018**, *127*, 1189–1197. https://doi.org/10.1016/j.ijheatmasstransfer.2018.07.155.
14. Cui, M.; Xu, B.B.; Lv, J.; Gao, X.W.; Zhang, Y. Numerical solution of multi-dimensional transient nonlinear heat conduction problems with heat sources by an extended element differential method. *Int. J. Heat Mass Transf.* **2018**, *126*, 1111–1119. https://doi.org/10.1016/j.ijheatmasstransfer.2018.05.100.
15. Adsul, P.P.; Dineshkumar, L. On code verification of 2D transient heat conduction in composite wall. *IOP Conf. Ser. Mater. Sci. Eng.* **2018**, *377*, 012128. https://doi.org/10.1088/1757-899X/377/1/012128.
16. Chiba, R. An Analytical Solution for Transient Heat Conduction in a Composite Slab with Time-Dependent Heat Transfer Coefficient. *Math. Probl. Eng.* **2018**, *2018*, 4707860. https://doi.org/10.1155/2018/4707860.
17. Del Cerro Velázquez, F.; Gómez-Lopera, S.A.; Alhama, F. A powerful and versatile educational software to simulate transient heat transfer processes in simple fins. *Comput. Appl. Eng. Educ.* **2008**, *16*, 72–82. https://doi.org/10.1002/cae.20159.
18. Janáčová, D.; Charvátová, H.; Kolomazník, K.; Fialka, M.; Mokrejš, P.; Vašek, V. Interactive software application for calculation of non-stationary heat conduction in a cylindrical body. *Comput. Appl. Eng. Educ.* **2013**, *21*, 89–94. https://doi.org/10.1002/cae.20453.
19. Herazo, R.E.D.; Quinones, L.G.O.; Ochoa, G.E.V. Development of an educational software in Matlab for transient heat transfer analysis. *Contemp. Eng. Sci.* **2017**, *10*, 953–961. https://doi.org/10.12988/ces.2017.79102.
20. Cantillo, L.M.; Quinones, L.O.; Ochoa, G.V. A Python based program for the parametric study of heat transfer processes in transient state. *Contemp. Eng. Sci.* **2017**, *10*, 1103–1111. https://doi.org/10.12988/ces.2017.79123.
21. Obregon, L.G.; Peralta, Y.Y.; Valencia, G.E. Parametric study of transient heat conduction on common geometrical configurations using a graphical user interface. *Chem. Eng. Trans.* **2018**, *70*, 2011–2016. https://doi.org/10.3303/CET1870336.
22. Strumłło, C.; Adamiec, J. Energy and quality aspects of food drying. *Dry. Technol.* **1996**, *14*, 423–448. https://doi.org/10.1080/07373939608917106.
23. Akter, F.; Muhury, R.; Sultana, A.; Deb, U.K. A Comprehensive Review of Mathematical Modeling for Drying Processes of Fruits and Vegetables. *Int. J. Food Sci.* **2022**, 2022. https://doi.org/10.1155/2022/6195257.
24. Kaya, A.; Aydin, O.; Dincer, I. Experimental and numerical investigation of heat and mass transfer during drying of Hayward kiwi fruits (*Actinidia deliciosa* Planch). *J. Food Eng.* **2008**, *88*, 323–330. https://doi.org/10.1016/j.jfoodeng.2008.02.017.
25. Sabarez, H.T. Computational modelling of the transport phenomena occurring during convective drying of prunes. *J. Food Eng.* **2012**, *111*, 279–288. https://doi.org/10.1016/j.jfoodeng.2012.02.021.
26. Lemus-Mondaca, R.A.; Zambra, C.E.; Vega-Gálvez, A.; Moraga, N.O. Coupled 3D heat and mass transfer model for numerical analysis of drying process in papaya slices. *J. Food Eng.* **2013**, *116*, 109–117. https://doi.org/10.1016/j.jfoodeng.2012.10.050.
27. Sabarez, H.T. Mathematical Modeling of the Coupled Transport Phenomena and Color Development: Finish Drying of Trellis-Dried Sultanas. *Dry. Technol.* **2014**, *32*, 578–589. https://doi.org/10.1080/07373937.2013.846366.
28. Kumar, C.; Joardder, M.U.H.; Farrell, T.W.; Karim, M.A. Multiphase porous media model for intermittent microwave convective drying (IMCD) of food. *Int. J. Therm. Sci.* **2016**, *104*, 304–314. https://doi.org/10.1016/j.ijthermalsci.2016.01.018.

29. Reddy, R.; Ravula, P.; Arepally, D.; Munagala, S.; Golla, S. Drying Kinetics and Modelling of Mass Transfer in Thin Layer Convective Drying of Pineapple. *Chem. Sci. Int. J.* **2017**, *19*, 1–12. https://doi.org/10.9734/csji/2017/32746.
30. Seyedabadi, E.; Khojastehpour, M.; Abbaspour-Fard, M.H. Convective drying simulation of banana slabs considering non-isotropic shrinkage using FEM with the Arbitrary Lagrangian–Eulerian method. *Int. J. Food Prop.* **2017**, *20*, S36–S49. https://doi.org/10.1080/10942912.2017.1288134.
31. Rahman, M.M.; Kumar, C.; Joardder, M.U.H.; Karim, M.A. A micro-level transport model for plant-based food materials during drying. *Chem. Eng. Sci.* **2018**, *187*, 1–15. https://doi.org/10.1016/j.ces.2018.04.060.
32. Yuan, Y.; Tan, L.; Xu, Y.; Yuan, Y.; Dong, J. Numerical and experimental study on drying shrinkage-deformation of apple slices during process of heat-mass transfer. *Int. J. Therm. Sci.* **2019**, *136*, 539–548. https://doi.org/10.1016/j.ijthermalsci.2018.10.042.
33. Boureima, D.; Thierry, K.Y.; Abdoulaye, C.; Hassim, G.; Salifou, O.; Joseph, B.D. Modeling of tomato convective drying with Comsol software. *Asian J. Sci. Technol.* **2019**, *10*, 10021–10028. Available online: http://www.journalajst.com (02.07.2024).
34. Rani, P.; Tripathy, P.P. Modelling of moisture migration during convective drying of pineapple slice considering non-isotropic shrinkage and variable transport properties. *J. Food Sci. Technol.* **2020**, *57*, 3748–3761. https://doi.org/10.1007/s13197-020-04407-4.
35. Turkan, B.; Etemoglu, A.B. Numerical investigation of wood drying. *Wood Res.* **2019**, *64*, 127–136.
36. Bergman, T.L.; Lavine, A.S.; Incropera, F.P.; Dewitt, D.P. *Fundamentals of Heat and Mass Transfer*, 7th ed.; John Wiley & Sons: Hoboken, NJ, USA, 2011; Volume 148.
37. Schneider, P.J. *Conduction Heat Transfer*; Addison-Wesley: Reading, MA, USA, 1957; pp. 9–48.
38. Langston, L.S. Heat Transfer from MultiDimensional Objects Using One Dimensional Solutions. *Int. J. Heat Mass Transf.* **1982**, *25*, 149–150.
39. Babakhani, J.; Veysi, F. Experimental study of geometric cuboid effect on convective heat transfer. *Eur. Phys. J. Plus* **2022**, *137*, 215. https://doi.org/10.1140/epjp/s13360-022-02430-2.
40. Ozalp, A.A.; Dincer, I. Hydrodynamic-thermal boundary layer development and mass transfer characteristics of a circular cylinder in confined flow. *Int. J. Therm. Sci.* **2010**, *49*, 1799–1812. https://doi.org/10.1016/j.ijthermalsci.2010.04.016.
41. Kaya, A.; Aydin, O.; Dincer, I. Heat and mass transfer modeling of recirculating flows during air drying of moist objects for various dryer configurations. *Numer. Heat Transf. Part A Appl.* **2008**, *53*, 18–34. https://doi.org/10.1080/10407780701557899.
42. Queiroz, M.R.; Nebra, S.A. Theoretical and experimental analysis of the drying kinetics of bananas. *J. Food Eng.* **2001**, *47*, 127–132. https://doi.org/10.1016/S0260-8774(00)00108-4.
43. Mousazadeh, S.M.; Shahmardan, M.M.; Tavangar, T.; Hosseinzadeh, K.; Ganji, D.D. Numerical investigation on convective heat transfer over two heated wall-mounted cubes in tandem and staggered arrangement. *Theor. Appl. Mech. Lett.* **2018**, *8*, 171–183. https://doi.org/10.1016/j.taml.2018.03.005.
44. Aral, S. Analysis of Mass And Heat Transfer Coefficients, Energy Consumption and Efficiency of in Dehydration of Cornelian Cherry. *Brill. Eng.* **2022**, *4*, 4742. https://doi.org/10.36937/ben.2022.4742.

Disclaimer/Publisher's Note: The statements, opinions and data contained in all publications are solely those of the individual author(s) and contributor(s) and not of MDPI and/or the editor(s). MDPI and/or the editor(s) disclaim responsibility for any injury to people or property resulting from any ideas, methods, instructions or products referred to in the content.